The *UARS* and EOS Microwave Limb Sounder (MLS) Experiments

J. W. WATERS, W. G. READ, L. FROIDEVAUX, R. F. JARNOT, R. E. COFIELD, D. A. FLOWER, G. K. LAU, H. M. PICKETT, M. L. SANTEE, D. L. WU, M. A. BOYLES, J. R. BURKE, R. R. LAY, M. S. LOO, N. J. LIVESEY, T. A. LUNGU, G. L. MANNEY, L. L. NAKAMURA, V. S. PERUN, B. P. RIDENOURE, Z. SHIPPONY, P. H. SIEGEL, AND R. P. THURSTANS

Jet Propulsion Laboratory, California Institute of Technology, Pasadena, California

R. S. HARWOOD, H. C. PUMPHREY, AND M. J. FILIPIAK

Department of Meteorology, Edinburgh University, Edinburgh, United Kingdom

(Manuscript received 2 September 1997, in final form 24 June 1998)

ABSTRACT

The Microwave Limb Sounder (MLS) experiments obtain measurements of atmospheric composition, temperature, and pressure by observations of millimeter- and submillimeter-wavelength thermal emission as the instrument field of view is scanned through the atmospheric limb. Features of the measurement technique include the ability to measure many atmospheric gases as well as temperature and pressure, to obtain measurements even in the presence of dense aerosol and cirrus, and to provide near-global coverage on a daily basis at all times of day and night from an orbiting platform. The composition measurements are relatively insensitive to uncertainties in atmospheric temperature. An accurate spectroscopic database is available, and the instrument calibration is also very accurate and stable. The first MLS experiment in space, launched on the (NASA) *Upper Atmosphere Research Satellite* (*UARS*) in September 1991, was designed primarily to measure stratospheric profiles of ClO, O_3, H_2O, and atmospheric pressure as a vertical reference. Global measurement of ClO, the predominant radical in chlorine destruction of ozone, was an especially important objective of *UARS* MLS. All objectives of *UARS* MLS have been accomplished and additional geophysical products beyond those for which the experiment was designed have been obtained, including measurement of upper-tropospheric water vapor, which is important for climate change studies. A follow-on MLS experiment is being developed for NASA's Earth Observing System (EOS) and is scheduled to be launched on the EOS CHEMISTRY platform in late 2002. EOS MLS is designed for many stratospheric measurements, including HO_x radicals, which could not be measured by *UARS* because adequate technology was not available, and better and more extensive upper-tropospheric and lower-stratospheric measurements.

1. Introduction

Microwave limb sounding obtains remote measurements of atmospheric parameters by observations of millimeter- and submillimeter-wavelength thermal emission as the instrument field of view (FOV) is scanned through the atmospheric limb from above. Development of the Microwave Limb Sounder (MLS) experiments began at the Jet Propulsion Laboratory (JPL) in the mid-1970s and included instruments deployed on aircraft (Waters et al. 1979; Waters et al. 1980) and balloons (Waters et al. 1981; Waters et al. 1984; Waters et al. 1988; Stachnik et al. 1992) prior to application of the technique from space. The measurement technique is described by Waters (1989, 1992a,b, 1993). Its features include 1) the ability to measure many atmospheric gases, with emission from molecular oxygen providing temperature and pressure; 2) measurements that can be made reliably, even in the presence of heavy aerosol, cirrus, or polar stratospheric clouds that can degrade ultraviolet, visible, and infrared techniques; 3) the ability to make measurements at all times of day and night and provide near-global coverage on a daily basis; 4) the ability to spectrally resolve emission lines at all altitudes, which allows measurements of very weak lines in the presence of nearby strong ones; 5) composition measurements that are relatively insensitive to uncertainties in atmospheric temperature; 6) a very accurate spectroscopic database; and 7) instrumentation that has very accurate and stable calibration, adequate sensitivity without necessarily requiring cooling, and provides good vertical resolution set by size of the antenna. New miniature integrated circuit technology for microwave radiometers (Weinreb 1997), now being studied for use in a future experiment, can provide good

Corresponding author address: Dr. J. W. Waters, Mail Stop 183-701, Jet Propulsion Laboratory, Pasadena, CA 91109.
E-mail: joe@mls.jpl.nasa.gov

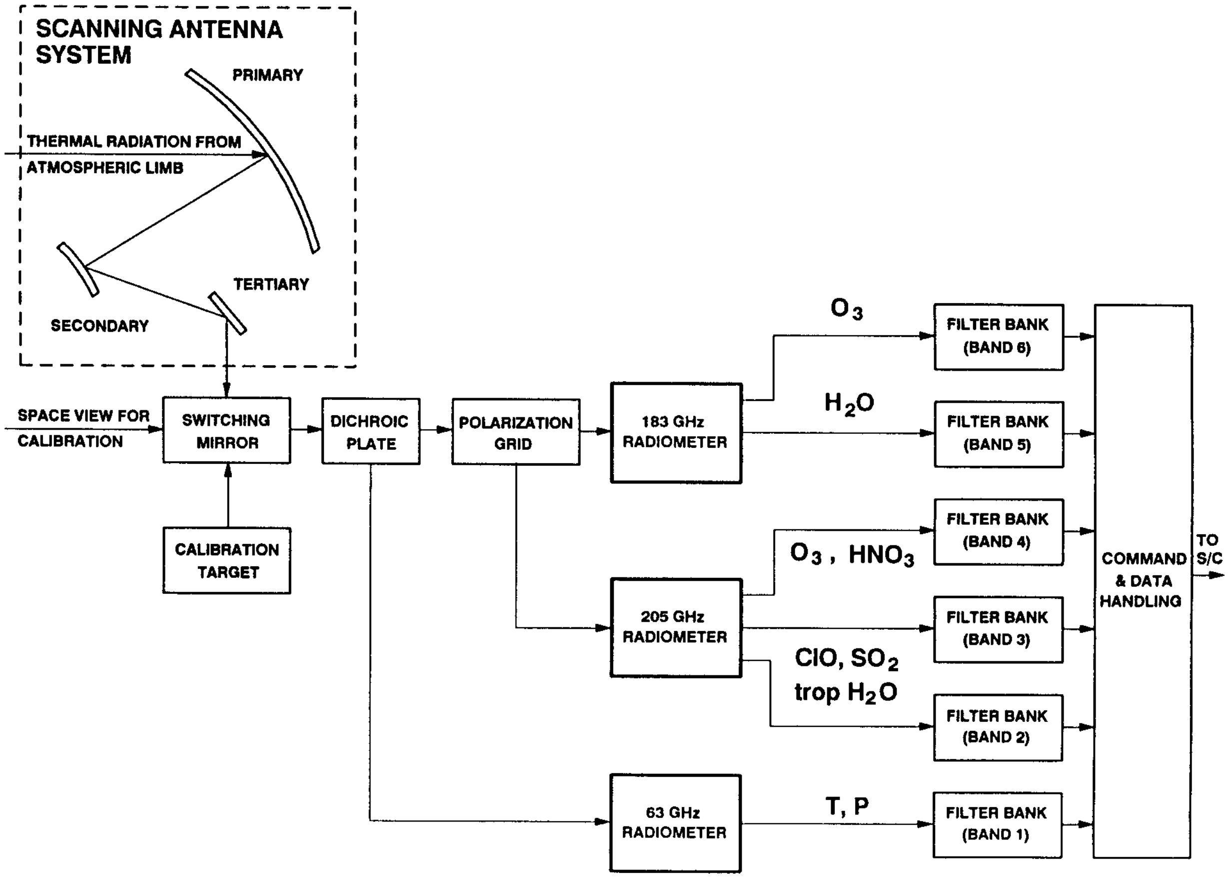

FIG. 1. Signal flow block diagram of the *Upper Atmosphere Research Satellite* (*UARS*) Microwave Limb Sounder (MLS) instrument.

horizontal resolution (including complete coverage between orbits) by allowing implementation of an array of radiometers with multiple FOVs simultaneously scanning the limb at different azimuth angles (Waters 1998).

Spectral line frequencies and strengths used for interpreting the MLS atmospheric measurements are available from the JPL Submillimeter, Millimeter, and Microwave Spectral Line Catalog (Pickett et al. 1992). Accuracy of line frequencies is typically seven digits or more and that of line strengths is typically four digits. The catalog database can be searched to ensure that all gases that might contribute significant amounts to the MLS signals are included in the data processing. Line-broadening parameters are obtained from laboratory measurements, for example, Pickett et al. (1981) and Oh and Cohen (1992, 1994), with uncertainties as low as ~3%. More laboratory measurements and better theoretical models of ''continuum absorption'' by water vapor and dry air would be helpful for improving the accuracy of MLS upper-tropospheric measurements.

2. The *UARS* Microwave Limb Sounder

a. Some general information on UARS *MLS*

The MLS launched 12 September 1991 on the *Upper Atmosphere Research Satellite* (*UARS*) (e.g., Reber 1993; Reber et al. 1993; Waters 1997; Dessler et al. 1998) is the first application of the microwave limb sounding technique from space. A somewhat similar experiment, the Millimeter-Wave Atmospheric Sounder has been flown on three space shuttle missions (Hartmann et al. 1996). The *UARS* MLS development was led by the California Institute of Technology Jet Propulsion Laboratory, with collaboration from Rutherford Appleton Laboratory, Heriot-Watt University, and Edinburgh University in the United Kingdom. The instrument (Barath et al. 1993) uses ambient-temperature double-sideband heterodyne radiometers that operate near 63 GHz (designed to measure stratospheric pressure, but also provide stratospheric temperature), 205 GHz (designed to measure stratospheric ClO, O_3 and H_2O_2), and 183 GHz (designed to measure stratospheric and mesospheric H_2O and O_3). A complete limb scan and radiometric calibration are performed every ~65 s during normal operations. Figure 1 shows a signal flow block diagram of the *UARS* MLS instrument. Calibration, described by Jarnot et al. (1996), is accurate to ~3% (3σ) overall in the most critical spectral bands. Lau et al. (1996) analyze the low-frequency 1/f noise of the instrument.

Figure 2 shows an example of spectra measured by

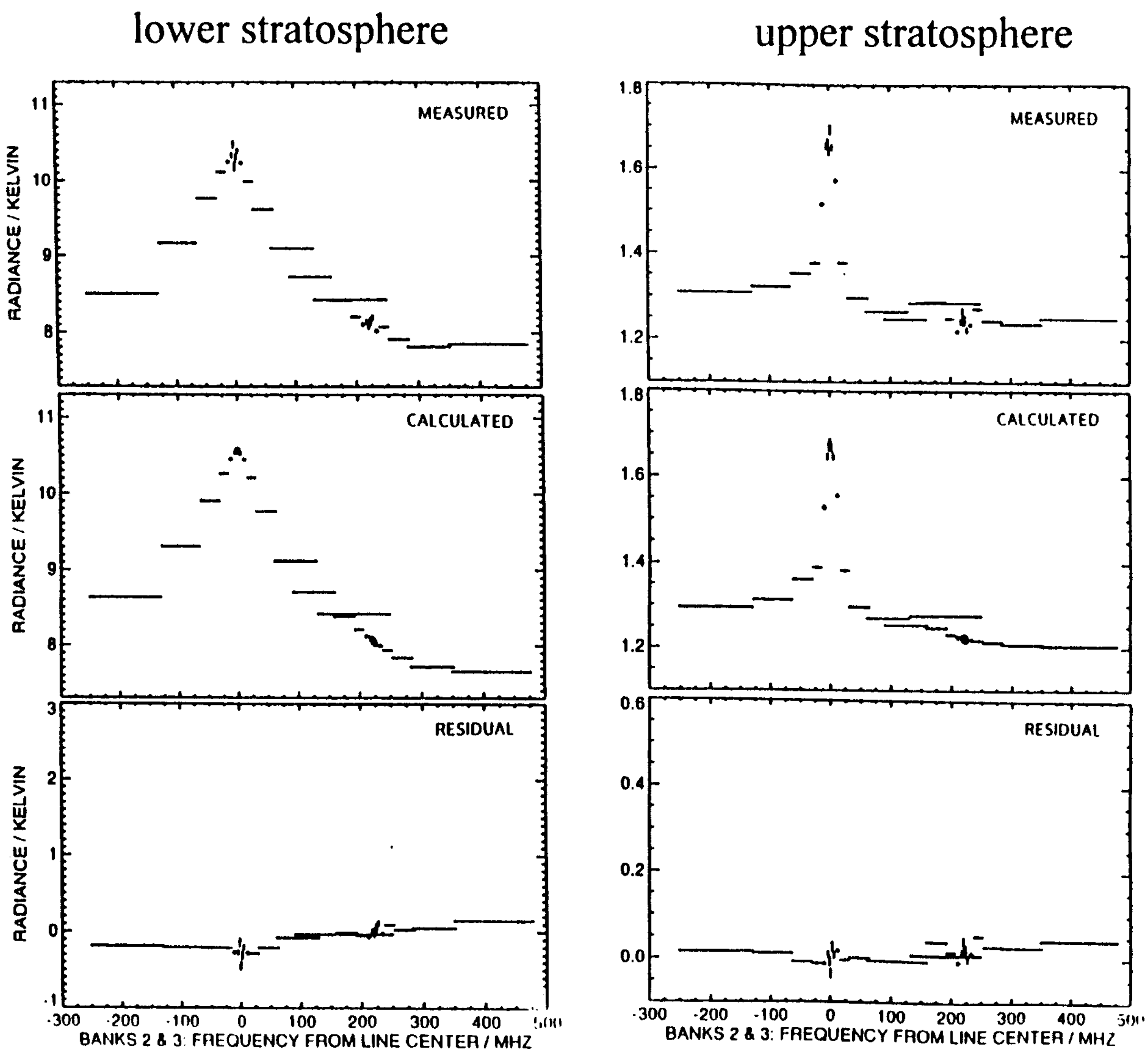

FIG. 2. ClO atmospheric thermal emission measured by *UARS* MLS and calculated from retrieved ClO vertical profiles (from Waters et al. 1996). The left panels are for lower-stratospheric ClO, where the tangent point of the MLS FOV was between 22- and 100-hPa tangent pressure, and the measured spectrum is the average of data from 16 daytime limb scans made in the Antarctic vortex on 16 August 1992. The right panels are for upper-stratospheric ClO, where the tangent point of the MLS FOV was between 2.2- and 10-hPa tangent pressure, and the measured spectrum is the average of 548 daytime limb scans made between 34°S and 80°N latitudes on 11 July 1993. The middle panels are the average of spectra calculated from individual ClO retrievals from these limb scans, and the bottom panels are the difference between measured and calculated. The horizontal bars indicate the spectral resolution of individual filters (all of which are sampled simultaneously) and the vertical bars indicate the expected noise in the average.

MLS and illustrates its ability to spectrally resolve individual emission lines. Having several spectral channels covering a single emission line, and resolving this line at all altitudes of interest, provides robust measurements since geophysical quantities can be obtained from the channel-to-channel spectrally varying component of the measured thermal emission. Extraneous effects, such as stray radiation, generally have spectrally flat emission over the spectral range used for measurements, and their uncertainties do not usually have first-order effects on the retrievals of geophysical parameters. Figure 3 shows 205-GHz radiances from the lower stratosphere measured by *UARS* MLS when the Tropics contained very heavy loading of aerosol from the Mount Pinatubo volcano. No effect of the aerosol on the MLS radiances is seen, as expected from theoretical considerations, with an observed upper limit of ~0.1%.

Validation of the MLS primary data products, and their accuracies and precisions, are described in a special issue of the *Journal of Geophysical Research* (volume 101, number D6, 30 April 1996) on *UARS* data evaluation: temperature/pressure by Fishbein et al. (1996); O_3 by Froidevaux et al. (1996), Cunnold et al. (1996a, b), and Ricaud et al. (1996); H_2O by Lahoz et al.

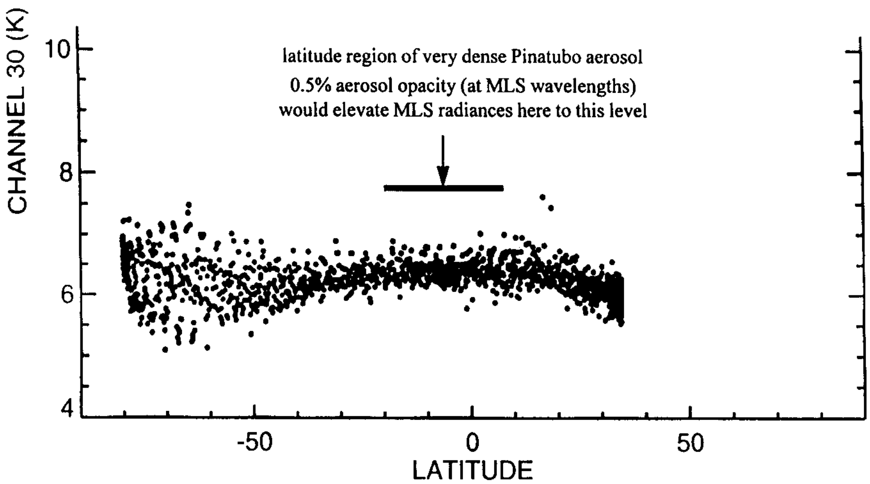

FIG. 3. MLS 205-GHz radiances (wing channel of ClO band) from the lower stratosphere (measurements interpolated to 50-hPa tangent pressure) vs latitude on 21 September 1991. The tropical lower stratosphere had very heavy loading of aerosol from the Pinatubo volcano at this time, but the MLS radiances are not noticeably affected by this aerosol layer, as expected, with an observational upper limit of ~0.1% opacity through the limb path.

(1996a); and ClO by Waters et al. (1996). Figure 4 shows the agreement obtained between MLS and some other well-calibrated measurements of the stratospheric O_3 profile. Additional results relevant to validation of these MLS measurements are included in Aellig et al. (1996), Crewell et al. (1995), Redaelli et al. (1994), Singh et al. (1996), and Wild et al. (1995). Although MLS was designed to include measurement of H_2O_2, this was predicated on stratospheric H_2O_2 being a major odd-hydrogen reservoir in the midstratosphere with predicted abundances of ~10 parts per billion by volume (ppbv) at the time of *UARS* MLS design. Refinements to parameters used for the theoretical predictions, and measurements (e.g., Chance et al. 1991), now indicate only ~0.1 ppbv H_2O_2 in the stratosphere; preliminary detection of a signal, corresponding to ~0.1 ppbv H_2O_2, has been obtained in averages of the MLS radiances (unpublished results). Additional data products obtained from *UARS* MLS, beyond that for which the instrument was primarily designed, include SO_2 injected into the stratosphere by the Pinatubo volcano (Read et. al. 1993), upper-tropospheric H_2O (e.g., Read et al. 1995), lower-stratospheric HNO_3 (Santee et al. 1995; Santee et al. 1997; Santee et al. 1998), temperature variances associated with atmospheric gravity waves in the stratosphere and mesosphere (Wu and Waters 1996a,b, 1997), detection of cirrus ice near the tropopause (D. L. Wu 1998, manuscript in preparation), and tentative measurement of stratospheric CH_3CN (N. J. Livesey 1998, manuscript in preparation). Fourier transform techniques applied to mapping MLS data are described by Elson and Froidevaux (1993). Figure 5 shows the vertical range of measurements published to date from *UARS* MLS. Recent work (D. L. Wu 1998, manuscript in preparation) has extended the temperature measurement upward to ~85 km altitude.

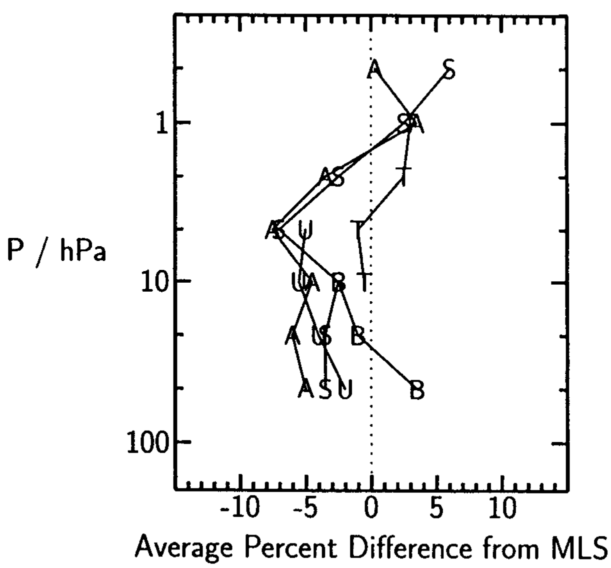

FIG. 4. Results of comparing MLS ozone with other well-calibrated near-coincident measurements (adapted from Froidevaux et al. 1996 and Cunnold et al. 1996a). Points A are the average differences of Stratospheric Aerosol and Gas Experiment (SAGE II) measurements selected in low aerosol situations, covering 25°–55°N latitudes, and made between September 1991 and December 1993. Points T are average differences of 295 Table Mountain (34°N), California, lidar profiles. Points B are average differences of 42 Boulder (40°N), Colorado, ozonesondes. Points U are average differences of eight balloon-borne ultraviolet photometer profiles, and points S are average differences of five balloon-borne SLS profiles.

UARS was designed for an 18-month duration mission, but at the time of writing, the MLS (along with most other *UARS* instruments) continues to operate after ~7 yr in orbit with no degradation in its 63- and 205-

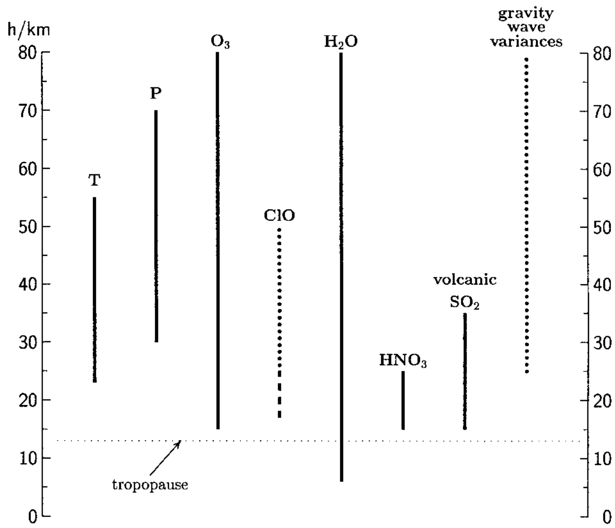

FIG. 5. Vertical range of published measurements obtained from *UARS* MLS. Solid lines indicate useful individual profiles. Dotted lines indicate zonal (or other) means, and the dashed line for ClO at lower altitudes indicates individual measurements when ClO is enhanced in the polar winter vortices. Additional measurements, not yet published, include cirrus ice near the tropopause, tentative detection of stratospheric CH_3CN and H_2O_2, and atmospheric temperature up to ~85 km.

GHz measurements except for time-sharing of these measurements with those of other *UARS* instruments due to decreases in power available from the spacecraft. The MLS 183-GHz radiometer failed in April 1993 after 18 months of excellent data had been obtained. The 63-GHz radiometer was turned off on 13 July 1997 to reduce MLS power consumption due to failure of a *UARS* battery; it has remained off to date (July 1998) with the tangent pressure information needed during data processing obtained from the measured 206-GHz ozone linewidth. Updated information can be obtained from the MLS Web site (http://mls.jpl.nasa.gov).

b. UARS *MLS results related to ozone loss in polar regions*

Early results from *UARS* MLS included the first maps of stratospheric ClO, the predominant form of chemically reactive chlorine involved in the destruction of stratospheric O_3, throughout the winter vortices of both the Antarctic and Arctic. Initial results (Waters et al. 1993a; Waters et al. 1993b; see also Chipperfield 1993) showed the lower-stratospheric Antarctic vortex to be filled with ClO in the region where O_3 was depleted, confirming earlier conclusions from ground-based and aircraft instruments that chlorine chemistry is the cause of the Antarctic ozone hole. They showed (Fig. 6) that ClO in the sunlit portion of the Antarctic vortex can become enhanced by June and that O_3 destruction by ClO is masked in the early Antarctic winter by influx of O_3 expected from diabatic descent. Enhanced ClO in the Antarctic vortex has been observed by MLS as early as late May to mid-June in each of its six years of operation to date; Fig. 7 shows maps for the earliest day each year when enhanced Antarctic ClO was observed by MLS. Recent analyses (Roscoe et al. 1997) of ground-based measurements and models also indicate Antarctic ozone loss starting in midwinter. Early MLS results showed that the Arctic winter lower-stratospheric vortex can also become filled with enhanced ClO, corresponding to calculated vortex-averaged O_3 destruction rates of ~0.7% per day. Filling, or near filling, of the lower-stratospheric Arctic winter vortex (as well as the Antarctic vortex) with enhanced ClO has been a recurrent feature observed by MLS over several years; Fig. 8 shows maps from selected days in the 1991–92 and 1996–97 winters. Results from 3D models (Douglass et al. 1993; Geller et al. 1993; Lefevre et al. 1994), produced shortly after the MLS results were obtained, showed the observed distribution and evolution of enhanced Arctic ClO were consistent with chemical-transport model predictions. The maximum ClO abundances reported from MLS, however, are slightly larger than predicted from the models (Lefevre et al. 1994; Lutman et al. 1997). Recent unpublished results indicate that MLS maximum values of enhanced lower-stratospheric ClO may be reduced slightly by retrievals with better vertical resolution, and this is currently under study.

A clear relationship was found between enhanced Arctic ClO observed by MLS and predicted polar stratospheric cloud formation along back trajectories associated with the enhanced ClO; sporadic large values of ClO seen by MLS outside the vortex were shown to be consistent with that expected to be caused by instrument noise (Schoeberl et al. 1993). Differences between the Arctic and Antarctic winter vortex conditions deduced from MLS observations are described by Santee et al. (1995), and deduced from combined MLS, CLAES (Cryogenic Limb Array Etalon Spectrometer; Roche et al. 1993), and HALOE (Halogen Occultation Experiment; Russell et al. 1993) data by Douglass et al. (1995). One difference between the Arctic and Antarctic is the decreased amount of HNO_3 in the Antarctic winter vortex relative to the Arctic, as shown in Fig. 9. HNO_3 provides a source of NO_x that quenches reactive chlorine, and the depletion of HNO_3 over Antarctica leads to longer duration of enhanced ClO and extended depletion of O_3 there. The smaller Antarctic abundances of HNO_3 can be traced to the lower temperatures and their longer duration in the Antarctic where polar stratospheric cloud particles containing HNO_3 can settle out of the stratosphere. Analyses of MLS HNO_3 observations through several Antarctic winters (Santee et al. 1998) have provided implications for processes related to formation of polar stratospheric clouds; they indicate that ternary solutions (Tabazadeh et al. 1994) play an important role. Analyses by Massie et al. (1997) of MLS, CLAES, and Improved Stratospheric and Mesospheric Sounder (Taylor et al. 1993) measurements over

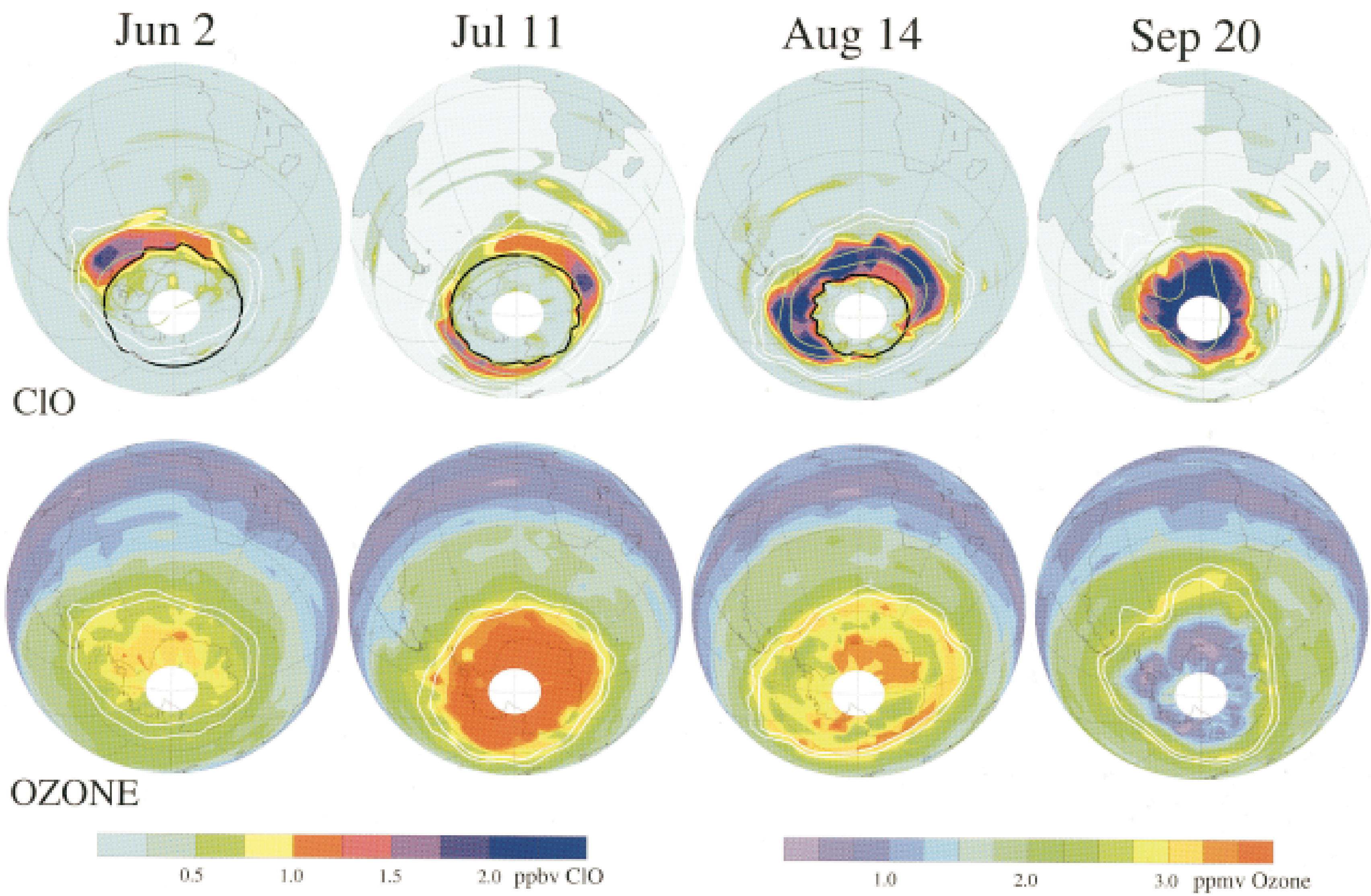

FIG. 6. ClO and ozone in the lower stratosphere through the Antarctic winter of 1992 (adapted from Waters et al. 1993a). The daily maps shown here are for MLS profiles interpolated to 465-K potential temperature (around 18-km altitude in the polar vortex). Irregular white contours are potential vorticity values (-2.5 and -3.0×10^{-5} K m^2 kg^{-1} s^{-1}, calculated from the U.S. National Centers for Environmental Prediction operational data), which indicate the approximate edge of the dynamical vortex, and the thin white contour concentric with the pole on the ClO maps is the edge of polar night. The white area poleward of 80° is where no measurements are obtained. The black contour of the ClO maps indicates the edge of daylight for the measurements, and thin green contours indicates temperatures of 190 and 195 K. Noise in the individual MLS ClO measurements at this altitude is $\sim$0.4 ppbv and the relatively isolated high values outside the polar vortex seen in this figure (as well as in following figures) are expected to be noise.

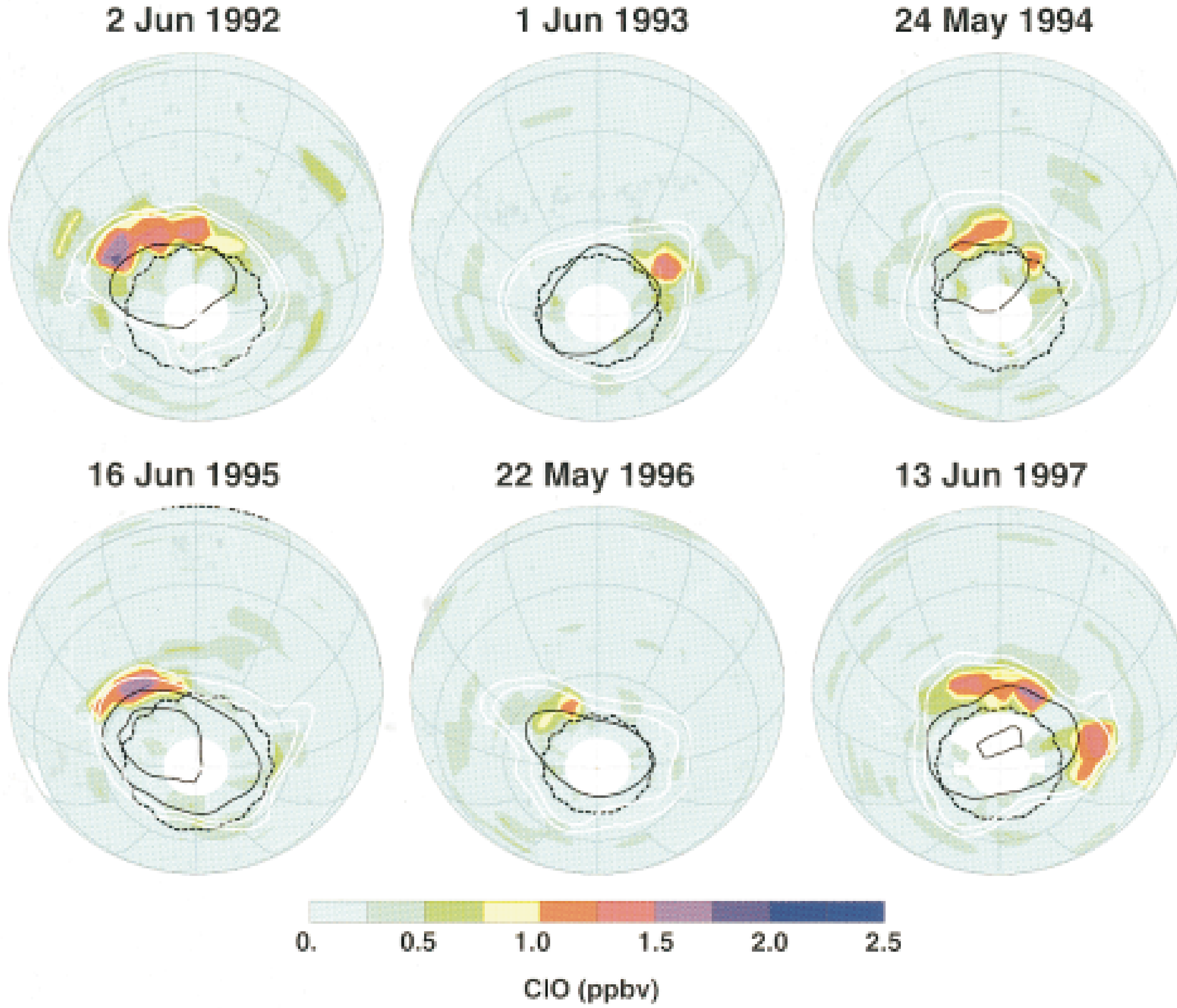

FIG. 7. MLS maps on the 465-K potential temperature surface for the earliest day each year on which MLS observed enhanced ClO in the Antarctic vortex. White contours are potential vorticity as in Fig. 6. The dashed curve is the edge of daylight for the measurements, and the solid black curves are temperatures of 195 and (when they exist) 188 K. These are not necessarily the earliest days each year Antarctic ClO was enhanced, just the earliest at which it was observed by MLS. Only in 1993 did MLS observations occur through the period of initial enhancement of Antarctic ClO; due to the *UARS* yaw state, or to operational constraints, observations in other years did not cover the period of transition to enhanced ClO. Differences from the 2 June 1992 ClO map in Fig. 6 are because MLS version 3 data are used in Fig. 6 whereas version 4 data are used here.

Scandinavia during 9–10 January 1991 imply initial polar stratospheric cloud (PSC) growth processes that transform sulfate droplets into ternary droplets or nitric acid dihydrate particles. A major question for future Arctic ozone loss is the extent to which the decrease in Arctic lower-stratospheric temperatures, possibly expected from increasing greenhouse gases, will lead to more Arctic ozone loss (due to strong nonlinear temperature dependence of the responsible mechanisms) even though stratospheric chlorine abundances should slowly start decreasing with the cessation in industrial production of source gases (e.g., Shindell et al. 1998; Salawitch 1998). Figure 10 compares conditions observed in the Arctic lower stratosphere on 20 February 1996 (one of the coldest days in the Arctic lower stratosphere during the period of MLS observations to date) with those observed in the Antarctic lower stratosphere on 30 August 1996. Similarities between the Arctic and Antarctic in regard to conditions affecting ozone depletion are evident.

Definitive loss of Arctic ozone due to chemistry associated with the enhanced ClO was determined from analyses of combined MLS and CLAES data by Manney et al. (1994). Bell et al. (1994) found the expected anticorrelation between enhanced Arctic ClO measured by MLS and HCl measured from the ground. Additional confirmation of the paradigm of chemical processing by polar stratospheric clouds leading to activation of strato-

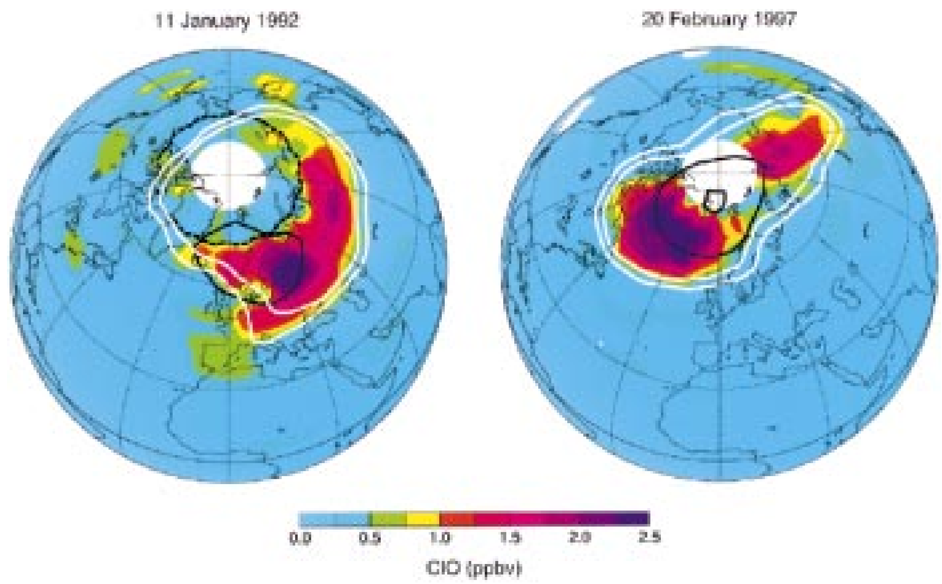

FIG. 8. MLS maps of lower-stratospheric ClO on 11 January 1992 (adapted from Waters et al. 1993b) and 20 February 1997 (adapted from Santee et al. 1997). These maps are for data interpolated to 465-K potential temperature. The white contours are potential vorticity values (2.5 and 3.0 $\times$ 10^{-5} K m^2 kg^{-1} s^{-1}), which indicate the approximate edge of the Arctic vortex. The dashed curve on the 11 January 1992 map marks the edge of daylight for the measurements, and the solid black curves are temperatures of 195 and (for the 20 February 1997 map) 188 K.

spheric chlorine is shown in the analyses of Northern Hemisphere CLAES, MLS, and HALOE data by Geller et al. (1995), and in Southern Hemisphere MLS and CLAES data by Ricaud et al. (1995; Ricaud et al. 1998). Mackenzie et al. (1996) compare lower-stratospheric vortex ozone destruction calculated from the MLS ClO with the MLS-observed change in O_3 for the northern winter of 1992–93 and southern winter of 1993. Additional comparisons between MLS observations and model results for polar chemistry are given by Eckman et al. (1995), Chipperfield et al. (1996), and Santee et al. (1996a). Schoeberl et al. (1996) use MLS, HALOE, and CLAES data in an analysis of the development of the Antarctic ozone hole. MLS measurements of Arctic ClO and O_3 for the six northern winters observed to date are described in the collective papers of Manney et al. (1994), Manney et al. (1995a), Manney et al. (1995b), Manney et al. (1996a), Manney et al. (1996b), Manney et al. (1997), Santee et al. (1995), Santee et al. (1996b), Santee et al. (1997), Waters et al. (1993b), and Waters et al. (1995). The largest vortex-averaged abundances of ClO in the Arctic and the largest Arctic ozone loss observed to date (through the 1997–98 northern winter) by MLS occurred in the 1995–96 winter (Manney et al. 1996b; Manney et al. 1997; Santee et al. 1996b; Manney et al. 1997). Low ozone ''pockets'' in the midstratospheric winter anticyclone have also been observed in MLS data and analyzed by Manney et al. (1995c), who show these cannot be explained solely by transport. Analyses by Nair et al. (1998) and Morris et al. (1998) indicate these pockets are formed when parcels of air are confined at high latitudes where odd-oxygen production is reduced and ozone relaxes to a lower photochemical equilibrium value.

c. UARS *MLS results related to high-latitude atmospheric dynamics*

MLS observations have been used in several studies to provide information on vortex and high-latitude dynamics. Harwood et al. (1993) studied the effects of the breakup of the Antarctic vortex on the water vapor distribution during September and November 1991 and, among other things, showed large parcels of air from the Antarctic vortex migrating to midlatitudes (Fig. 11). Manney et al. (1993) describe the evolution of ozone observed by MLS in relation to the Antarctic polar vortex in August and September 1992, and Fishbein et al. (1993) analyze waves seen in MLS observations of stratospheric temperature and ozone during this period. Lahoz et al. (1993) and Lahoz et al. (1994) use MLS H_2O, CLAES N_2O, and U.K. Meteorological Office data to study the evolution of midstratospheric water vapor and vortex processes in the Northern Hemisphere winter of 1991–92; Lahoz et al. (1996b) do a similar study for the Southern Hemisphere winter of 1992. Manney et al. (1995d) and Manney et al. (1995e) compare Lagrangian transport calculations with MLS observations of H_2O and O_3, and CLAES observations of N_2O and CH_4. Morris et al. (1995) apply a trajectory mapping technique to compare MLS and HALOE water vapor measurements and analyze dynamical wave-breaking

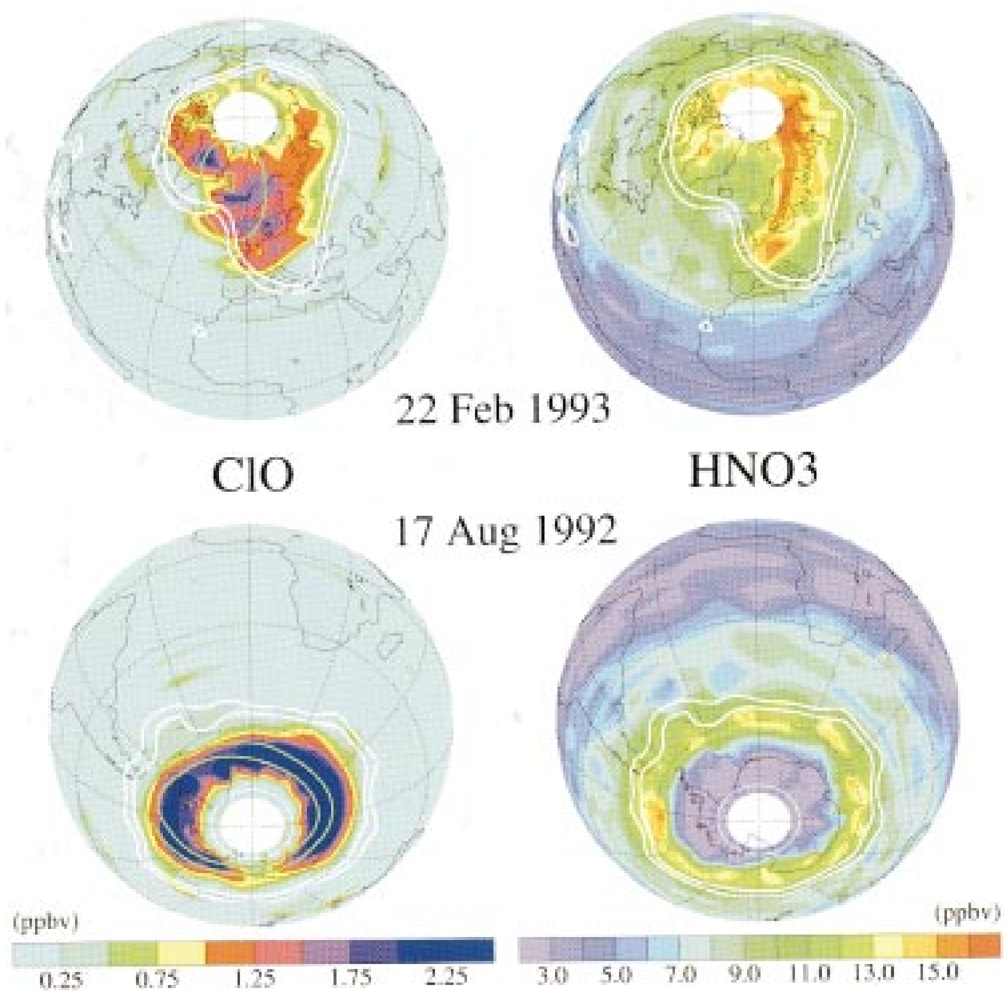

FIG. 9. MLS maps of lower-stratospheric ClO and HNO_3 on 22 February 1993 (top) and 17 August 1992 (bottom) comparing Arctic and Antarctic ClO and HNO_3 (adapted from Santee et al. 1995). The data are interpolated to 465-K potential temperature and white irregular contours are of potential vorticity, as in Figs. 6 and 8, which indicate the approximate edge of the polar vortices. The thin white contour concentric with the south pole is the edge of polar night, and green contours on the ClO maps indicate temperatures of 195 and 188 K.

events. Orsolini et al. (1997), Orsolini et al. 1998), and Manney et al. (1998a) use MLS O_3 data to initialize a high-resolution transport model and analyze ozone laminae along the Arctic polar vortex edge seen in lidar and ozonesonde data.

d. UARS *MLS results related to global distributions and variations of atmospheric parameters*

An overview of zonal mean O_3 results from the first two-and-a-half years of MLS operation is given by Froidevaux et al. (1994); in addition to features observed in stratospheric O_3, this work includes initial results of examining residual differences between the stratospheric O_3 column from MLS and the total O_3 column from the Total Ozone Mapping Spectrometer (TOMS), with information on tropospheric ozone as the ultimate goal. Analyses by Ziemke et al. (1996) using these datasets have shown zonal asymmetries in Southern Hemisphere column ozone that have implications of biomass burning. Elson et al. (1994) describe large-scale variations observed in MLS O_3, and Elson et al. (1996) show zonal and large-scale variations in MLS H_2O. Pumphrey and Harwood (1997) analyze MLS radiance data to obtain information on variations of H_2O and O_3 throughout the mesosphere and show that H_2O in the mesosphere is transported mainly by advection. Future processing of MLS data will use nonlinear retrieval algorithms for H_2O, which should improve the standard MLS H_2O product, especially in the mesosphere and lower stratosphere (Pumphrey 1998). Mote et al. (1998) use results from these prototype nonlinear retrievals to analyze subseasonal variations in tropical lower-stratospheric water vapor. Morrey and Harwood (1998) analyze the version 4 MLS water vapor and see major interhemispheric differences in lower-stratospheric water vapor content of

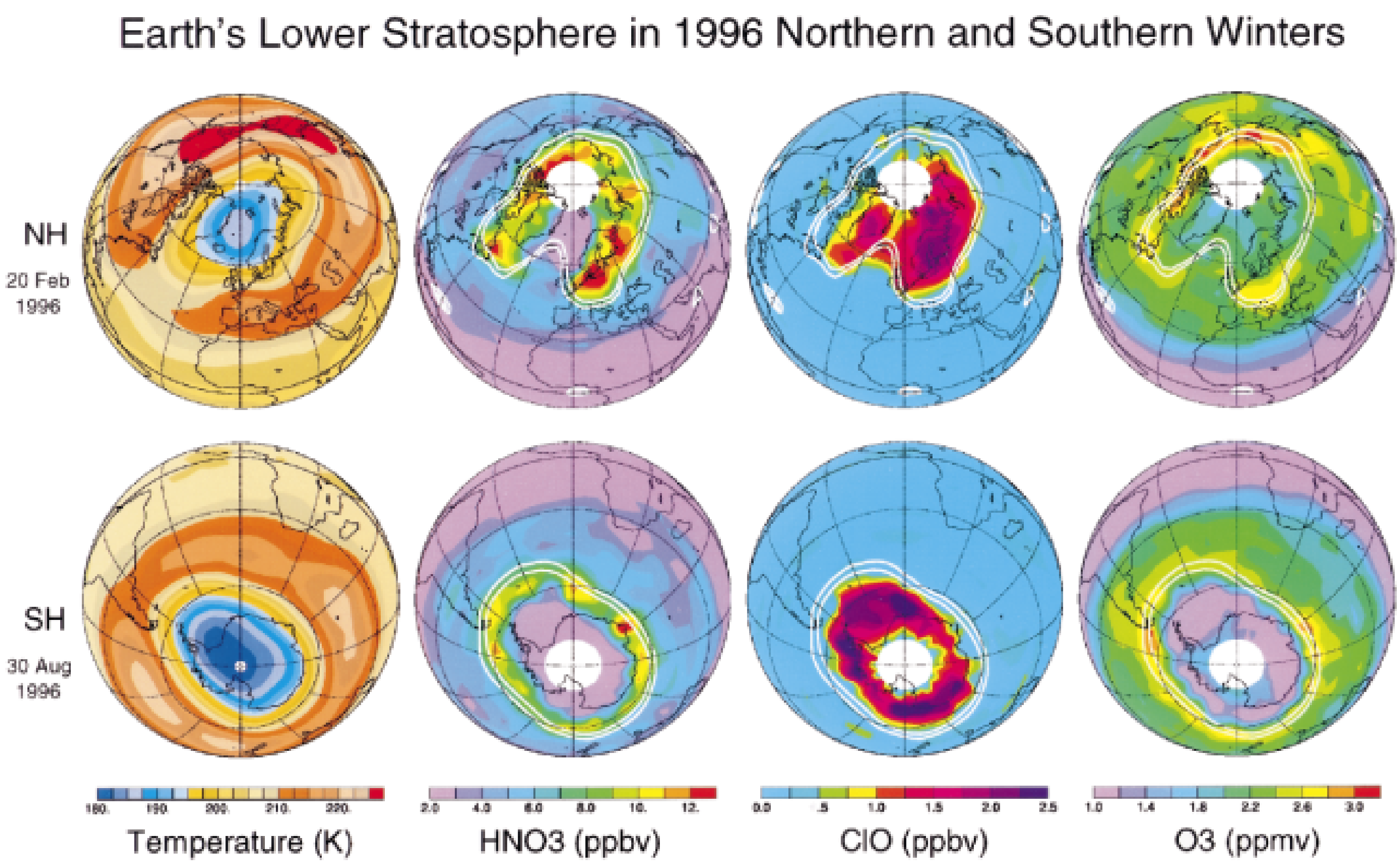

FIG. 10. The earth's lower stratosphere in the Northern Hemisphere on 20 February 1996 (top) and in the Southern Hemisphere on 30 August 1996 (bottom). Measurements interpolated to the 465-K potential temperature surface, as in previous figures with white contours indicating potential vorticity values representative of the polar vortex edge, are shown here. The HNO_3, ClO, and O_3 data are from *UARS* MLS, and the temperature data are from operational analyses of the U.S. National Centers for Environmental Prediction. Temperatures in the blue and violet color ranges allow formation of polar stratospheric clouds from HNO_3 and H_2O; heterogeneous chemistry on these clouds leads to enhanced ClO, which causes chemical destruction of O_3. The amount of ozone destruction each winter in the polar vortices depends on the duration of ClO enhancement, which is longer for the Antarctic than the Arctic. This difference is traceable to the Antarctic lower stratosphere being colder, and remaining cold for longer, than the Arctic.

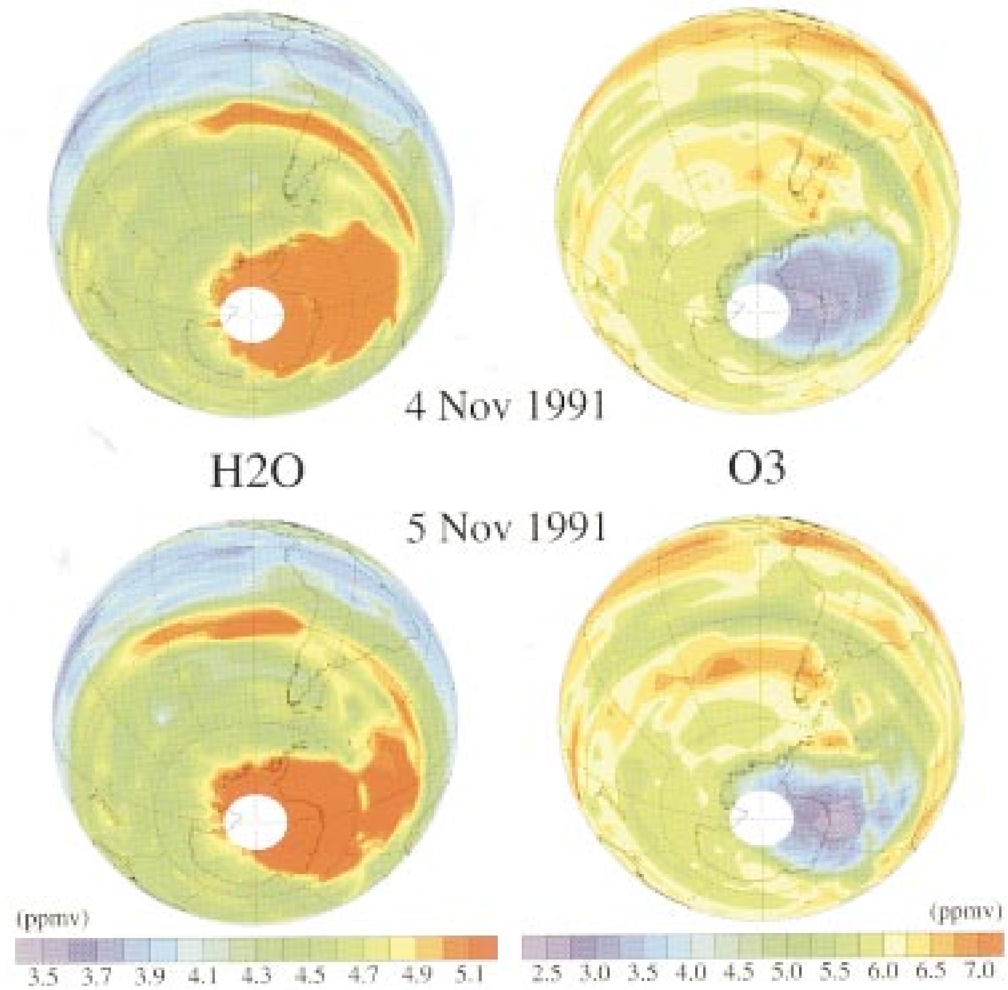

FIG. 11. MLS maps of water vapor and ozone at 655-K potential temperature (~25 km) on 4 and 5 November 1991 (adapted from Harwood et al. 1993).

the winter polar vortices, as expected, but at midlatitudes find only small interhemispheric differences that are not strongly related to the dehydration of the Antarctic vortex. Randel et al. (1995) include MLS and HALOE data in analyzing changes in stratospheric ozone following the Pinatubo eruption. Randel et al. (1998) analyze seasonal cycles and quasi-bienniel oscillation variations in HALOE data, using water vapor data from MLS to fill in winter polar latitudes where HALOE data are not available. Dessler et al. (1995) found that incorporation of O_3 measured by MLS into chemical relationships improved comparison between predicted correlations of HCl and $ClONO_2$ and those measured by HALOE and CLAES. Chandra et al. (1996) use MLS data in examining ozone variability in the upper stratosphere during the declining phase of solar cycle 22. Hood and Zhou (1998) use MLS ozone and temperature data, and *UARS* Solar-Stellar Irradiance Comparison Experiment (Rottman et al. 1993) solar ultraviolet data, to analyze the stratospheric effects of 27-day solar ultraviolet variations.

The zonal mean latitudinal distribution of ClO observed by MLS in the upper stratosphere (Fig. 12; see also Waters et al. 1996; Jackman et al. 1996) shows a minimum at low latitudes as expected (Solomon and Garcia 1984) from increased quenching by larger amounts of upper-stratospheric CH_4 at low latitudes, which is due to rising motion in the Tropics transporting CH_4 from lower altitudes. As shown in Fig. 12, the upper-stratospheric ClO minimum moves northward in northern summer, qualitatively tracking the seasonal variation in CH_4 (Kumer et al. 1993), which follows the rising motion in the Tropics. Explanation of the ~0.1 ppbv difference in upper-stratospheric ClO for the two periods shown here is under investigation. Eckman et al. (1995) found that quantitative agreement of theoretical model predictions with MLS upper-stratospheric ClO measurements is substantially improved by includ-

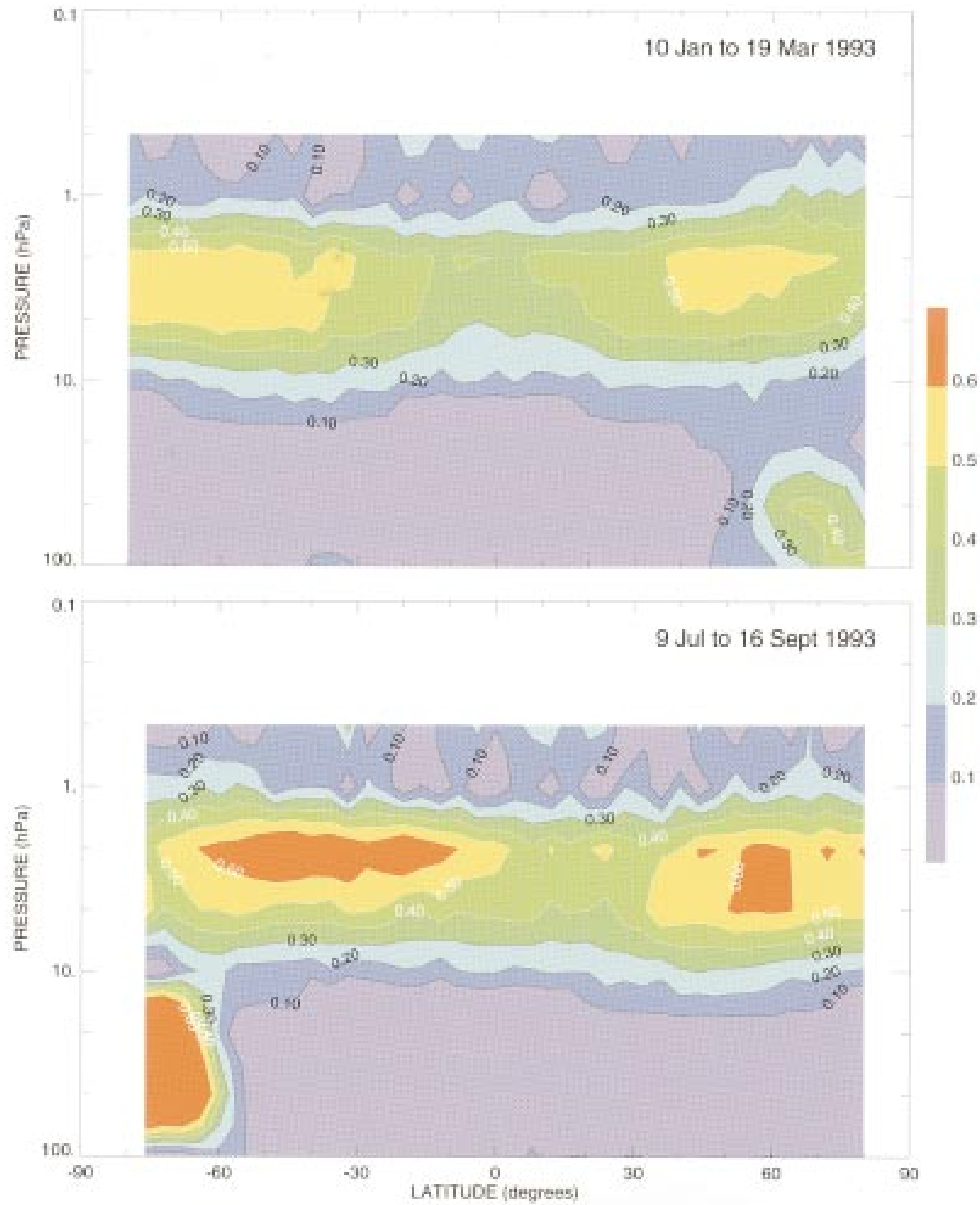

FIG. 12. Zonal mean daytime ClO from MLS for January–March 1993 (top) and July–September 1993 (bottom). The color bar is in parts per billion.

ing 5% branching of the reaction OH + ClO to HCl + O_2, consistent with a conclusion on this reaction reached earlier by Toumi and Bekki (1993) with regard to matching the Submillimeter Limb Sounder (SLS) measurements of upper-stratospheric ClO and HCl (Stachnik et al. 1992). Laboratory confirmation of the OH + ClO reaction with ~6% yield of HCl has now been obtained (Lipson et al. 1997). Dessler et al. (1996a) used MLS ClO measurements, along with CLAES $ClONO_2$ and HALOE NO_2, to test predictions of chlorine partitioning between ClO and $ClONO_2$. Dessler et al. (1996b) also used MLS ClO, and HALOE and CLAES NO_2, to examine implications for the model ''ozone deficit'' in the upper stratosphere. Khosravi et al. (1998) found a significant reduction in the ozone deficit by analyses that used *UARS* data (MLS ClO and HALOE NO_x, H_2O and CH_4) and a 3D model. Considine et al. (1998) analyze interhemispheric asymmetry in the upper-stratospheric

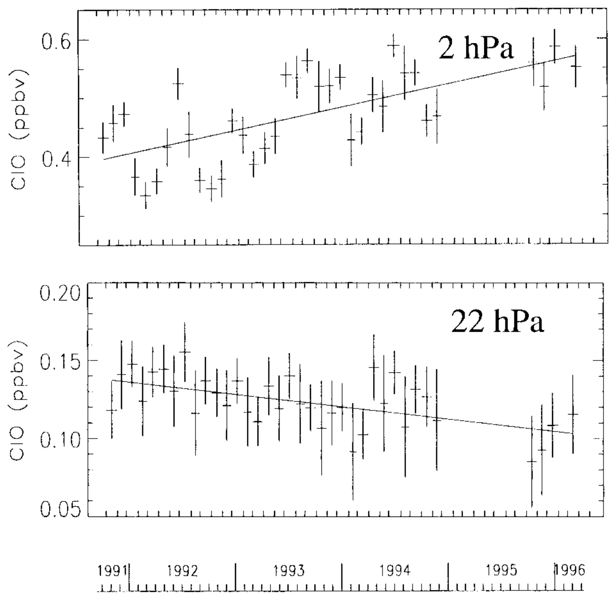

FIG. 13. ClO trends observed by MLS at 2 (top) and 22 hPa (bottom). These data (crosses) are zonal averages for 30°S–30°N latitudes and the slanted straight lines are fits to the data (adapted from L. Froidevaux et al. 1998, unpublished manuscript).

ozone trend using an interactive zonal mean model and *UARS* data, whereas the model produces interhemispheric asymmetry in the trend as seen in solar backscattered ultraviolet observations, analysis of MLS ClO does not show the asymmetry required for the model explanation. An increasing trend in upper-stratospheric ClO, expected from increasing abundances of stratospheric chlorine, and a decreasing trend in lower-stratospheric ClO, expected from changes in heterogeneous chemistry during the fallout of Pinatubo aerosols, has been detected in MLS data (L. Froidevaux 1998, unpublished manuscript), as shown in Fig. 13.

Two-day waves in the stratosphere have been analyzed by Limpasuvan and Leovy (1995) using MLS H_2O data, and by Wu et al. (1996) using MLS temperatures. Four-day waves observed in MLS ozone, temperature, and geopotential height have been analyzed by Allen et al. (1997) and, in the new nonlinear prototype H_2O data, by Manney et al. (1998b). MLS data have been used in calculations of stratospheric residual circulation by Rosenlof (1995) and Eluszkiewicz et al. (1996). Huang et al. (1997) analyze ozone diurnal variations observed by MLS.

e. UARS *MLS results related to the Tropics*

Kelvin waves observed in MLS tropical data have been analyzed by Canziani et al. (1994), Canziani et al. (1995), and Stone et al. (1995), and MLS observations of the semiannual oscillation have been analyzed by Ray et al. (1994). Randel et al. (1993) describe CLAES and MLS observations of stratospheric transport from the Tropics to midlatitudes by planetary wave mixing. Carr et al. (1995) performed initial analyses of MLS tropical stratospheric H_2O data, and Mote et al. (1995) found variations in these data that could be related to the annual cycle in tropical tropopause temperatures. More extensive analyses by Mote et al. (1996), greatly aided by the use of *UARS* HALOE H_2O and CH_4, confirmed that tropical air entering the stratosphere from below is marked by its tropopause water vapor mixing ratio and retains a distinct memory of tropical tropopause conditions for 18 months or more; this analysis implies that vertical mixing is weak and that subtropical stratospheric ''transport barriers'' are effective at inhibiting transport into the Tropics. Schoeberl et al. (1997) also use MLS and other *UARS* data to estimate the dynamical isolation of the tropical lower stratosphere. Wu et al. (1998) study the equatorial diurnal tide in the stratosphere using MLS temperature data and the Canadian Middle Atmosphere Model.

f. UARS *MLS measurements of upper-tropospheric water vapor*

Knowledge of upper-tropospheric water vapor and its variations is very important for understanding feedback mechanisms associated with climate change. Although not designed for this measurement, the MLS ClO band is very sensitive to upper-tropospheric water vapor when its FOV is scanned down through the troposphere, which happens on each limb scan. Features of the *UARS* MLS upper-tropospheric water vapor measurements include the ability to observe through cirrus, to determine vertical structure with more than 1300 profiles per day, and to obtain measurements at all times of day and night. The measurement is obtained from continuum emission (in contrast to well-defined spectral line emission for other MLS measurements) and currently relies upon empirical expressions for absorption coefficients describing the continuum emission from water vapor and dry air near 203 GHz (Read et al. 1995); these expressions are thought accurate to ~20%. Effects of cirrus ice on the water vapor measurement are generally expected to be less than ~20% at 215 hPa (Read et al. 1995). Initial results, primarily at 215 hPa (Read et al. 1995), showed that scientifically useful measurements can be produced, and interesting atmospheric features have been observed in this preliminary dataset. The data were found reasonably consistent with coincident aircraft measurements (Newell et al. 1996a) and with the expected tropical Walker circulation (Newell et al. 1996b). A preliminary upper-tropospheric water vapor ''climatology'' from MLS has been compared with that of high thick cloud (Read et al. 1995). Synoptic-scale features have been observed; one over the east coast of the United States during March 1993 has been compared with independent results from the Goddard Space Flight Center data assimilation model and good qualitative agreement obtained (Read et al. 1995; Rood et al. 1997). See Chen

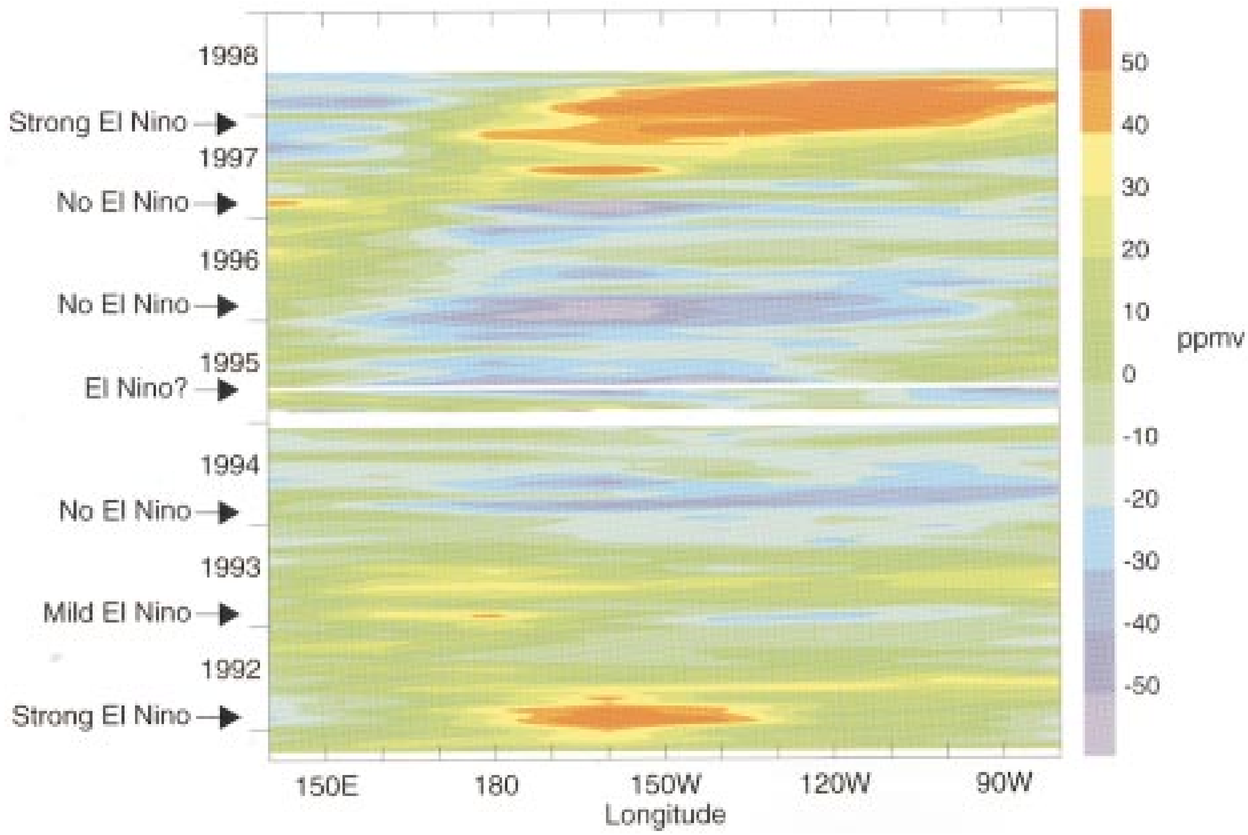

FIG. 14. Tropical Pacific upper-tropospheric water vapor anomalies observed by MLS. These data show deviations from the mean of the preliminary retrievals of 215-hPa water vapor from *UARS* MLS. Measurements made within 5° of the equator were included in this plot, and the data have been temporally smoothed with a Gaussian having 1-month width. Labels along the left axis indicate whether or not an El Niño event occurred that year. Note the large increases in upper-tropospheric water vapor during the 1991–92 and, especially, the 1997–98 El Niño events.

et al. (1998) for further comparisons between data assimilation model results and *UARS* MLS observations. Elson et al. (1996) applied spectral analyses to examine the time evolution of MLS zonal mean data and deviations from the zonal mean. Stone et al. (1996) used MLS upper-tropospheric H_2O measurements to investigate the structure and evolution of eastward-traveling medium-scale wave features in the Southern Hemisphere summertime; they found results consistent with paradigms for the structure and evolution of baroclinic disturbances. Haas and Pfister (1998) use MLS (and other) data in a site survey for the future airborne Stratospheric Observatory for Infrared Astronomy.

Clark et al. (1998) analyzed variability of MLS upper-tropospheric H_2O tropical data and found an intraseasonal cycle with a period of 30–85 days evident in the western Pacific; this cycle is associated with eastward-propagating disturbances of zonal wavenumbers 1–2, suggesting it is related to the Madden–Julian oscillation (Madden and Julian 1971). Newell et al. (1997) found variations in MLS tropical upper-tropospheric H_2O over the 1991–94 period to be closely related to sea surface temperature variations in the eastern tropical Pacific, at both seasonal and interannual timescales. Figure 14 shows temporal and longitudinal variations observed in MLS upper-tropospheric H_2O over the tropical Pacific for measurements made from start of mission in late September 1991 through 1 June 1998. Anomalies associated with El Niño sea surface temperature disturbances in 1991–92 and, especially, in 1997–98 are clearly evident in these data. Hu and Liu (1998) use the MLS data to analyze the impact of upper-tropospheric humidity on the midlatitude greenhouse effect.

An improved MLS upper-tropospheric water vapor dataset (with retrievals at 147, 215, 316, and 464 hPa, and values available both as mixing ratio and relative humidity with respect to ice) has recently been produced for the entire *UARS* mission. Figure 15 gives ''curtain plots'' made from these data that show the vertical variation along the measurement track for one day's observations; interesting features are observed and some of these are discussed in the figure caption. Quantitative validation of this dataset is now under way (W. G. Read 1998, manuscript in preparation). Sandor et al. (1998) use the new data in their analyses of the seasonal behavior of tropical to midlatitude upper-tropospheric wa-

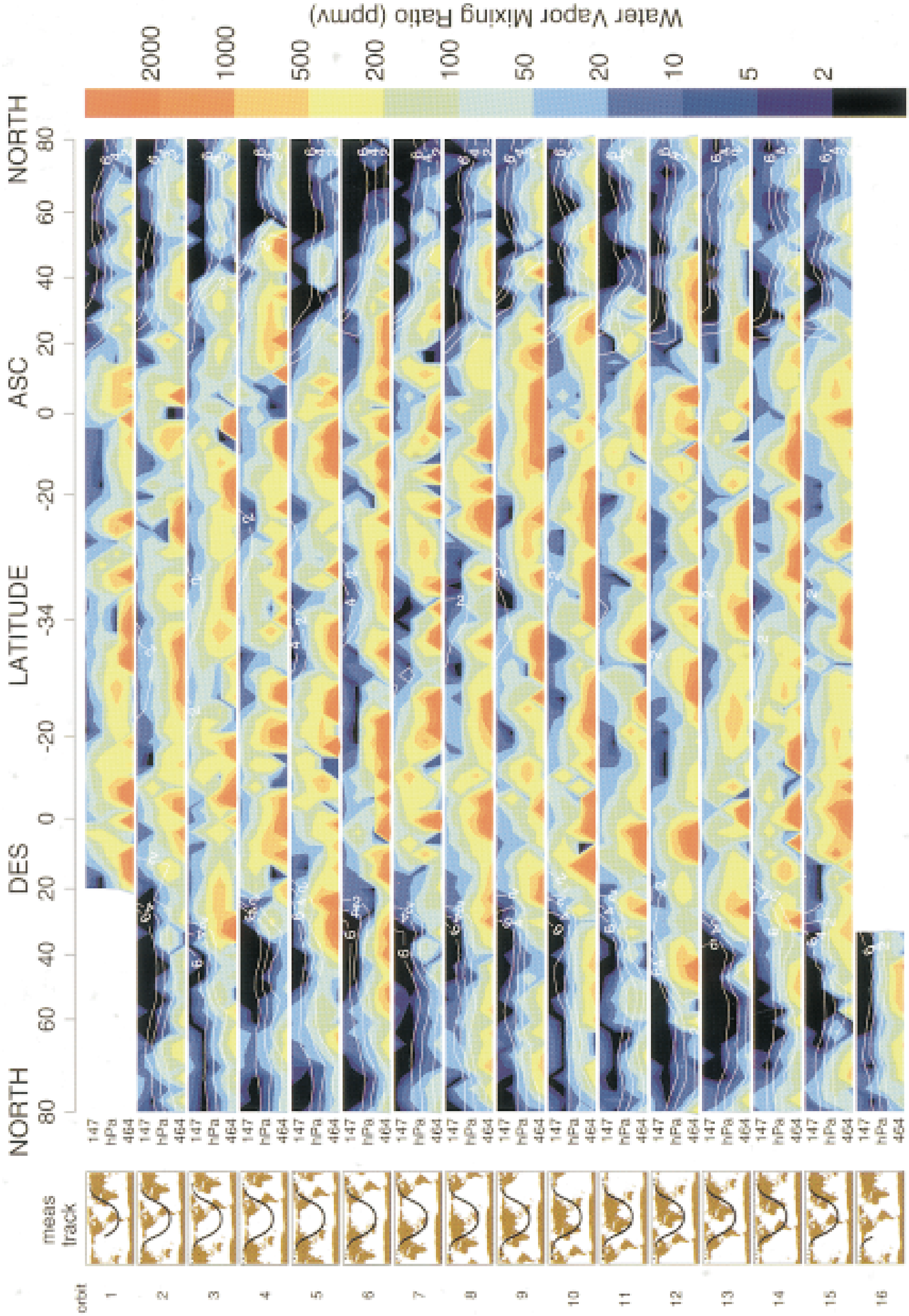
Water Vapor Mixing Ratio (ppmv)
2000
1000
500
200
100
50
20
10
5
2
NORTH
ASC
LATITUDE
DES
NORTH
80
60
40
20
0
-20
-34
-20
0
20
40
60
80
147
hPa
464
meas
track
orbit
1
2
3
4
5
6
7
8
9
10
11
12
13
14
15
16

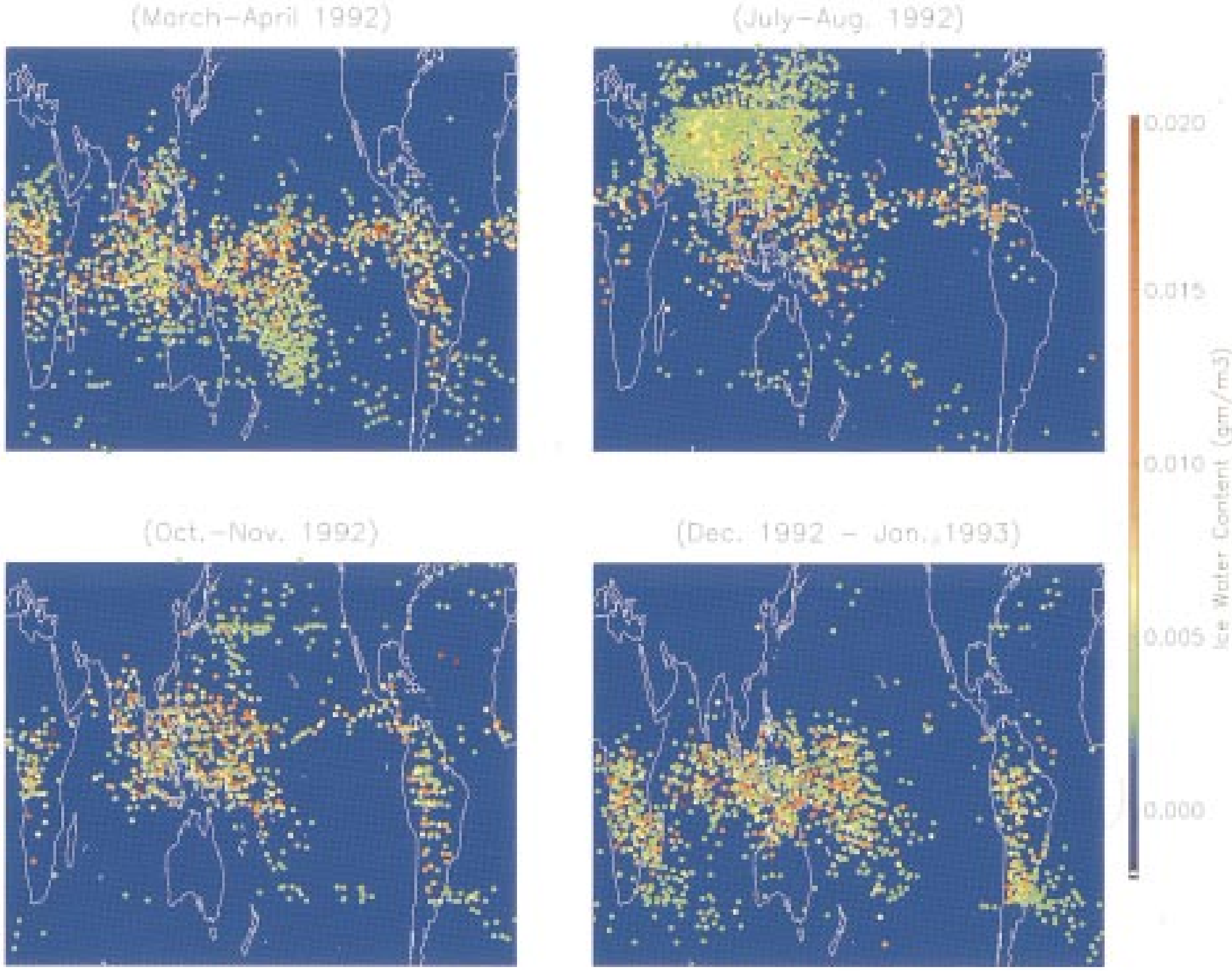

FIG. 16. Some initial results of cloud ice at 100 hPa retrieved from *UARS* MLS radiances at 186 and 203 GHz (adapted from D. L. Wu et al. 1998, manuscript in preparation) assuming no scattering, which corresponds to assuming a negligible number of particles larger than ~100 μm. The four panels are for different seasons as indicated, and values indicated by the colored dots are the total ice content within the MLS observation volume, ~3 km (vertical) by ~300 km (horizontal along the line of sight) by ~30 km (horizontal orthogonal to the line of sight), reported as average ice density over this volume.

←

FIG. 15. Results for one day from an improved *UARS* MLS upper-tropospheric water vapor dataset, recently made available for the entire *UARS* mission and currently undergoing validation, which has retrieval points at 147, 215, 316, and 464 hPa in the vertical. Data from each orbit are displayed in separate horizontal panels with the measurement tracks (which descend from 80°N to 34°S latitude and then ascend back to 80°N) and orbit numbers for the day indicated at the left. The horizontal axis of each panel is distance along the measurement track, with corresponding latitudes given at the top of the figure. The vertical axis is logarithm of atmospheric pressure where pressure ranges between 464 hPa at the bottom of each panel to 147 hPa at the top. Colors show the retrieved water vapor mixing ratio in parts per million by volume, on an approximately logarithmic scale given by the color bar at right. White contours give potential vorticity values of (2, 4, 6) $\times 10^{-6}$ K m^2 kg^{-1} s^{-1} calculated from the U.S. National Centers for Environmental Prediction (NCEP) operational data; the contour labeled 2 is an approximate indication of the tropopause. These results are for 14 March 1993 (Greenwich day) when an intense blizzard was near the east coast of the United States, and the tropopause along the coast was as low as ~500 hPa (Read et al. 1995; Rood et al. 1997). This low tropopause, indicated both by water vapor from MLS and by potential vorticity calculated from NCEP data, can be seen in the vertical structure of measurement tracks shown here: around 30°–40°N on the ascending (right) portion of orbit 5 and the descending (left) portion of orbit 13. The ''Pacific event'' on this day highlighted in Fig. 5 of Rood et al. (1997) is evident around 40°–50°N in the ascending portion orbit 11 where measurements are along the northeast coast of Asia, and at successive lower latitudes in ascending portions of earlier orbits where measurements cross a narrower arm of the feature extending nearly to Hawaii (see bottom panel of Fig. 4 in Read et al. 1995 and Fig. 5b of Rood et al. 1997); this event may not be so evident in earlier versions of the MLS data.

ter vapor and find seasonally adjusted humidity to be higher in the Northern Hemisphere than at equivalent Southern Hemisphere latitudes. They also find the peak of the frequency distribution of MLS tropical measurements at ~200 and ~300 hPa to be much drier than mean and median values, and that values of this peak are drier in the tropical wet than dry season at ~300 hPa in agreement with analyses of other datasets by Spencer and Braswell (1997) and Chiou et al. (1997). However, the MLS data at ~150 hPa (where publications using the other datasets do not report results) show values of this peak that are wetter in the tropical wet season than in the dry season, and this new result may have important implications for feedback mechanisms affecting climate variability.

Related to upper-tropospheric water vapor, *UARS* MLS also has the potential to provide information on upper-tropospheric cloud ice. Ice and water vapor can be distinguished by their different effects on MLS observations near 186 and 203 GHz, and signatures characteristic of ice emission are seen in the data (D. L. Wu 1998, manuscript in preparation). Under the assumption that the ice particles are smaller than ~100 μm (i.e., much smaller than the ~1.5-mm wavelength of the observations) and no liquid water is present, the emission signal is dependent to first order upon the total ice content within the field of view and is relatively insensitive to the particle size distribution. Measurements can then be easily converted to ice content, and Fig. 16 gives maps of preliminary results for 100-hPa altitude and different seasons. The largest observed upper-tropospheric ice abundances are associated with regions of greatest deep convection (e.g., the tropical west Pacific, landmasses in summer, and the Indian monsoon), as expected. More work is needed (and is under way) to understand the capability and limitations of MLS emission measurements of upper-tropospheric cloud ice and to extract information from scattering signals (e.g., Evans and Stephens 1995; Evans et al. 1998), which are seen in the data at lower altitudes where larger particles and more effects of scattering are expected. Additional data on the statistics of ice particle sizes at various altitudes in the upper troposphere and lower stratosphere would be helpful for interpreting the MLS measurements.

g. UARS *MLS results for atmospheric gravity waves*

Analyses of the 63-GHz radiances from MLS have produced the first global maps of atmospheric temperature variances at ~100 km horizontal scales associated with gravity wave activity in the stratosphere and mesosphere (Wu and Waters 1996a,b, 1997). These analyses use measurements made near the bottom of each limb scan where all spectral channels in the MLS 63-GHz band measure optically thick radiances; in this situation the different individual channels sense different altitudes (essentially independent of the limb scan angle) depending upon the atmospheric optical depth, which varies with the channel spacing from spectral line center, and a vertical profile is obtained for each 2 s measurement—with better horizontal resolution (but coarser vertical resolution) than obtained by the ''conventional'' limb sounding used for other MLS measurements. The results provide information on gravity waves with spatial scales of ~30–100 km in the horizontal and greater than ~10 km in the vertical. The mapped variances show high correlation with regions of strong background winds that are expected to play a major role in determining gravity wave amplitudes in the stratosphere and mesosphere. The observed variance grows exponentially with height in the stratosphere but exhibits near-zero growth in the mesosphere as might be expected from wave breaking and dissipation at the higher altitudes. The data also show correlation with surface topography features and regions of tropospheric convective activity, which are expected sources of gravity waves. Analysis by Alexander (1997) indicates that the MLS maps are consistent with model predictions of atmospheric gravity wave behavior but that the dominant patterns in the maps can be explained by the Doppler-shifting effects of background winds on the gravity wave spectrum, without requiring any geographical variation in the sources. The extent to which MLS can provide information on atmospheric gravity wave sources is a current topic of investigation. Preliminary results by C. McLandress (1998, personal communication) appear promising in regards to the MLS data providing quantitative information on the longitudinal variation of gravity wave sources in the summer subtropics.

h. UARS *MLS results for SO_2 injected into the stratosphere by volcanoes*

Starting within 10 days of launch, and continuing for approximately two months, MLS observed the three-dimensional distribution and decay of residual SO_2 injected into the stratosphere by the Mount Pinatubo eruption that occurred about three months before launch of *UARS.* These observations (Read et al. 1993) showed the Pinatubo SO_2 mixing ratio maximum to occur around 26-km altitude with abundances of ~15 ppbv on 21 September 1991. The observed SO_2 decay has *e*-folding times of 29 days at 26 km and 41 days at 21 km, consistent with expectations that the primary destruction of SO_2 is due to reaction with OH leading to formation of stratospheric sulfate aerosols. Projected backward to time of eruption, the total amount of SO_2 injected by Pinatubo is estimated from MLS data to be 17 MT, consistent with estimates inferred from other measurements. SO_2 injected into the stratosphere by the South American Lascar volcano was also detected by MLS on 21 and 22 April 1993 (unpublished results).

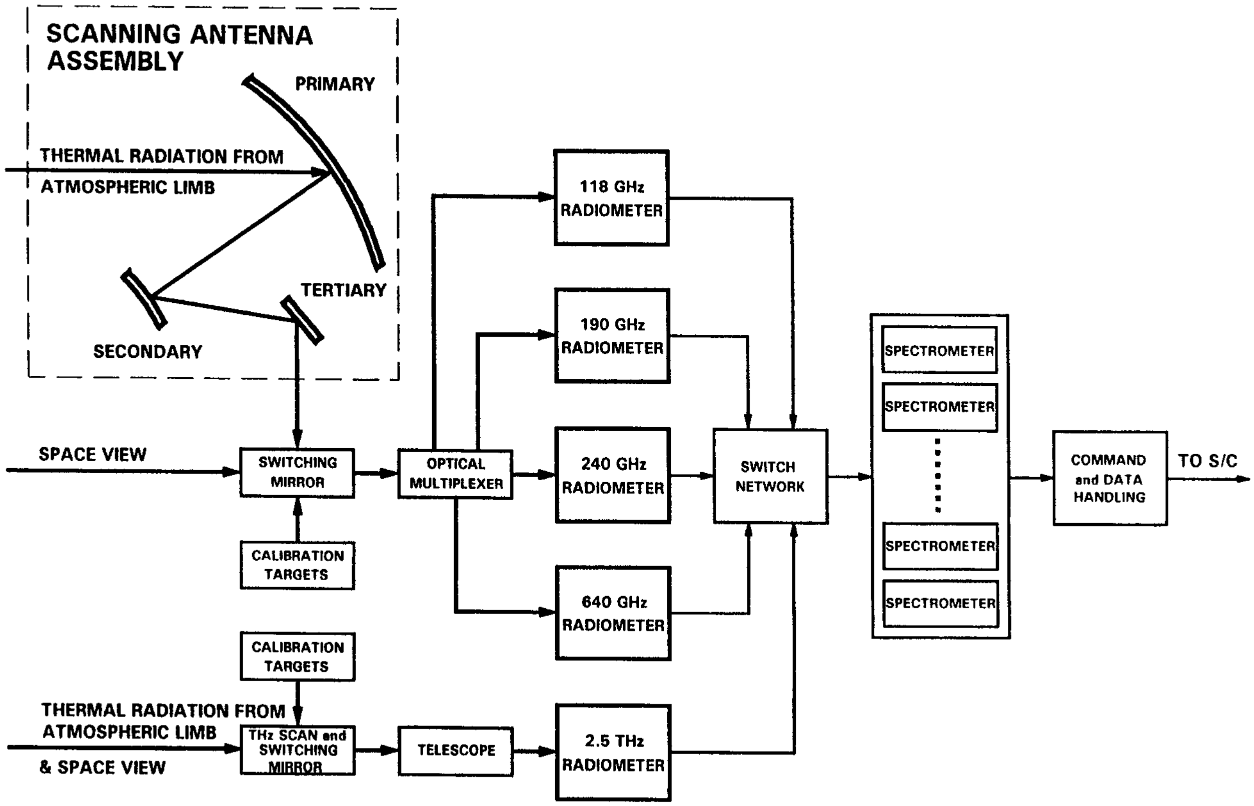

FIG. 17. Signal flow diagram for the Earth Observing System Microwave Limb Sounder (EOS MLS) instrument.

3. The Earth Observing System (EOS) MLS

a. Some general information on EOS MLS

The Earth Observing System (EOS) MLS is scheduled for launch on the EOS CHEMISTRY mission at the end of 2002. The EOS MLS instrument will be improved over *UARS* MLS in providing 1) more and better upper-tropospheric and lower-stratospheric measurements, 2) additional stratospheric measurements for chemical composition and long-lived dynamical tracers, 3) better global coverage and spatial resolution, and 4) better precision for many measurements. These improvements are possible because of 1) advances in microwave technology that provide measurements to higher frequencies where more molecules have spectral lines and spectral lines are stronger, and provide greater instantaneous spectral bandwidth for measurements at lower altitudes; 2) a better understanding of the capabilities of the measurement technique as a result of the *UARS* experience; and 3) the EOS near-polar (98° inclination, sun synchronous) orbit that allows nearly pole-to-pole coverage on each orbit, whereas the *UARS* orbit (57° inclination) and its precession forces MLS to switch between northern and southern high-latitude measurements on an approximate monthly basis, and critical periods are often missed. EOS MLS observes in the orbital plane (looking forward), which provides latitude coverage between 82°S and 82°N on each orbit, whereas *UARS* MLS looks to the side in a direction 90° to the satellite velocity vector. The EOS MLS measurement geometry also allows better information to be obtained along the measurement track: there is some overlap in the atmospheric paths of adjacent limb scans, and this is used to advantage in determining variations in geophysical parameters along the measurement track.

EOS MLS has radiometers in spectral bands centered near 118, 190, 240, 640, and 2500 GHz. The radiometers incorporate advanced technology, including planar-technology mixers (Siegel et al. 1993) and monolithic millimeter-wavelength integrated-circuit amplifiers (Weinreb et al. 1997) as the first stage at 118 GHz. Figure 17 shows a signal flow block diagram for EOS MLS, and Fig. 18 shows the spectral bands it measures. The radiometers and spectral bands for EOS MLS were chosen for minimizing the overall complexity of an instrument to produce the needed measurements and to provide some limited measurement redundancy (which also gives a quality check on the measurements). Vertical resolution of the measurements is generally ~2–3 km, although this will vary depending upon signal-to-noise ratio for the particular measurement and there are tradeoffs between vertical resolution and precision. Useful upper-tropospheric water vapor measurements, for example, are expected with ~1 km vertical resolution.

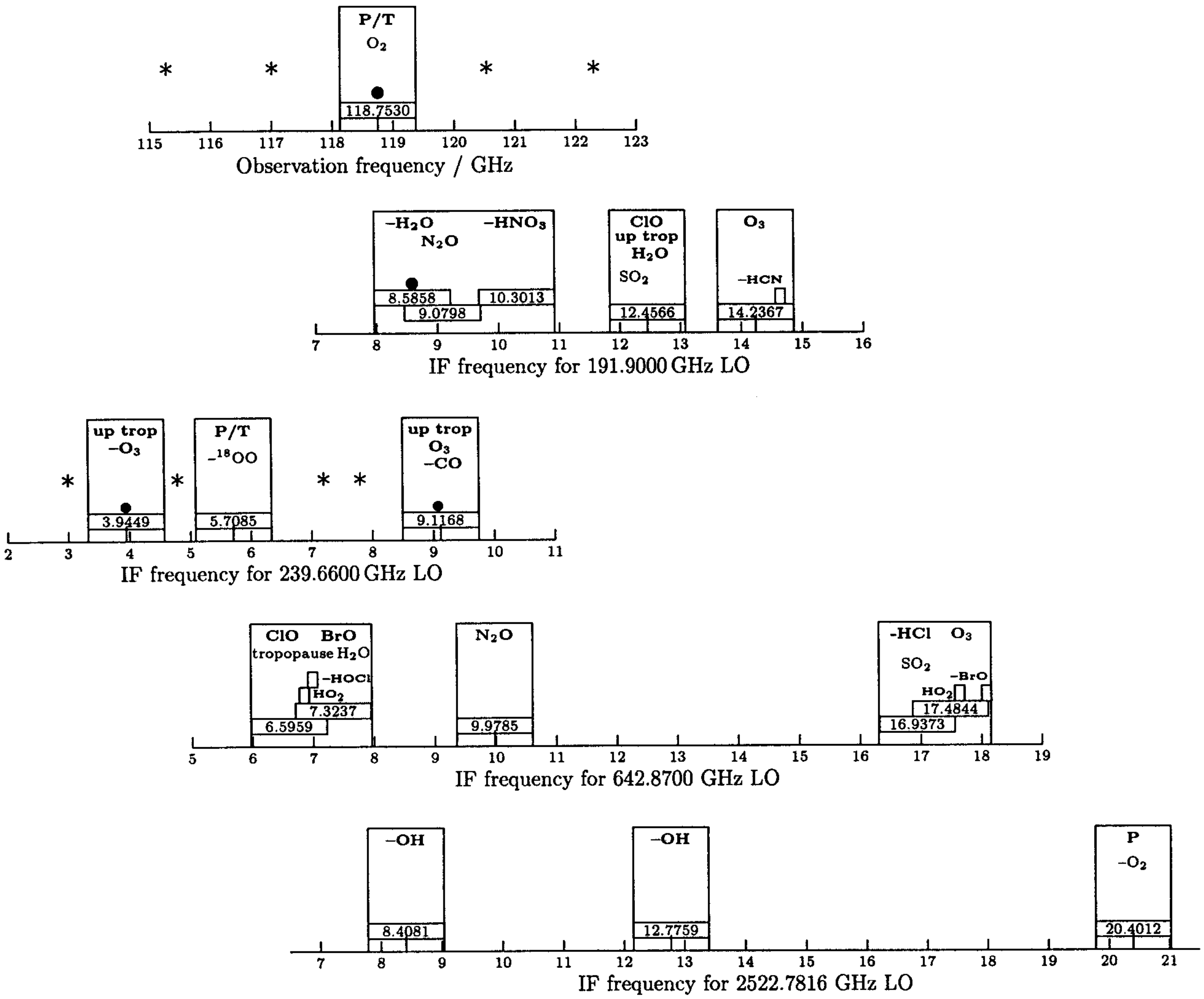

FIG. 18. EOS MLS spectral bands. The EOS MLS radiometers, except that operating near 118 GHz, are double sideband (having approximately equal responses from intermediate frequencies, IFs, above and below the local oscillator, LO, frequency). The spectral bands in the IF frequencies of these radiometers are shown here, and each band contains a multifrequency filter bank spectrometer. The primary targeted molecule is indicated for each band, and a minus sign in the molecular symbol indicates the spectral line appears in the lower sideband of the radiometer. Asterisks indicate locations of additional broadband individual filters, and bullets indicate locations of spectrometers with high spectral resolution for mesospheric signals. Numbers inside boxes indicate the IF frequencies of spectrometers that are centered on spectral lines of target molecules, and include the effects of orbital motion Doppler shifts.

Each EOS MLS limb scan, under nominal operation, will be performed approximately every 1.5° great circle along the orbital track (about 165 km distance and 25 s in time), which is ~3× more dense than on *UARS* MLS. The nominal scan range will be from ~2 to ~60 km above the earth's surface, and an individual measurement integration time is ~0.16 s. The vertical scan is programmable and alternative scan patterns can be chosen to provide more intense measurements of certain altitude regions or to provide measurements at higher altitudes in the mesosphere and lower thermosphere. Figure 19 shows the suite of measurements planned from each of the EOS MLS radiometers.

b. EOS MLS measurements for stratospheric chemistry

EOS MLS will provide key measurements throughout the stratosphere to test our understanding of its chemistry and provide new insights and early detection of changes. The lower-stratospheric measurements are particularly important since they will occur when 1) lower-stratospheric ozone, especially in the Arctic, is vulnerable to increased depletion due to effects of small decreases in temperature and potential changes in other parameters such as an increase in H_2O; 2) stratospheric chlorine loading is at or near its maximum; and 3) some recovery of ozone at low altitudes in the Antarctic ozone

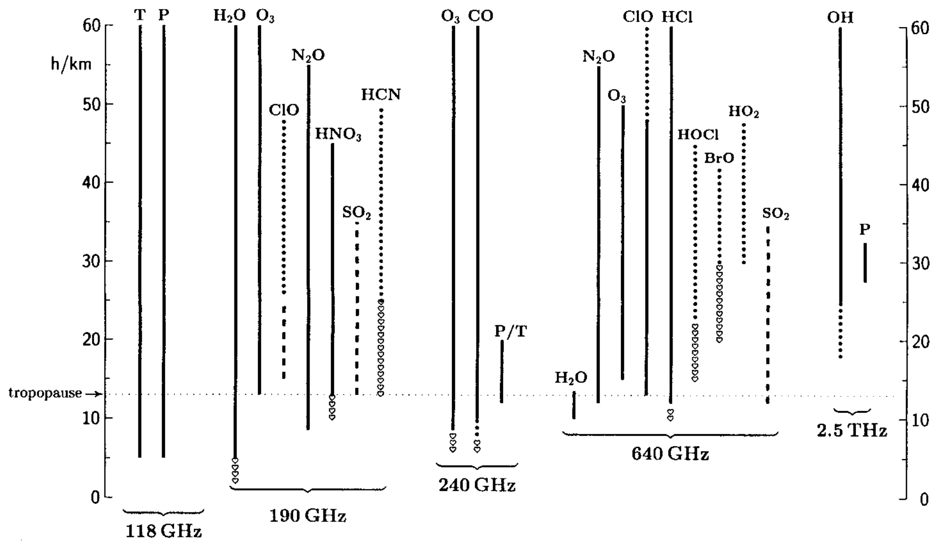

FIG. 19. EOS MLS measurements. Solid lines indicate useful individual profiles. Dotted lines indicate zonal (or other) means. Dashed lines indicate volcanic SO_2 and enhanced ClO. Hearts indicate measurement goals.

hole might be detectable in the later portion of the mission (Hofmann 1996) to verify that CFC regulations are having the expected effect.

The simultaneous and commonly calibrated MLS measurements of ClO, HNO_3, H_2O, HCl, N_2O, O_3, and temperature provide a powerful suite to improve understanding of key processes that could lead to greater ozone loss in the Arctic and to provide diagnostics of observed ozone loss. ClO abundances allow estimates of the amount of ozone loss due to chlorine chemistry. Abundances of HNO_3 and H_2O, and temperature, critically affect the microphysics leading to formation of surfaces upon which heterogeneous chemistry can occur and convert chlorine from reservoir to reactive forms. Abundances of HNO_3 also affect the rate at which reactive chlorine is converted back to reservoir forms. Measurements of N_2O, a long-lived tracer, help separate chemical and dynamical causes of observed changes. Measurements of OH, HO_2, BrO, and HOCl, along with those mentioned above, will improve our understanding of tropical and midlatitude stratospheric ozone changes. The suite of measurements includes key species in the HO_x and ClO_x cycles now thought to dominate tropical and midlatitude lower-stratospheric ozone loss. The ability of MLS to observe through dense aerosol will be critical for monitoring stratospheric chemistry after any volcanic eruptions that cause large increases in stratospheric aerosol loading.

The EOS MLS measurements of stratospheric OH will fill a serious gap in global observations to date because, as stated in the report of a workshop on ''Atmospheric Trace Gas Measurement for the Year 2000 and Beyond,'' published in the January/February 1995 issue of the National Aeronautics and Space Administration EOS publication *The Earth Observer,* 1) OH controls the conversion of CH_4 to H_2O, 2) reactions of HO_x radicals are the most important loss mechanisms for ozone in both the lowest and highest regions of the stratosphere, 3) reactions with OH control the rate of oxidation of sulfur gases (SO_2, OCS) to sulfate aerosol, and 4) OH is in competition with heterogeneous chemistry in controlling the transfers between radical species in both the NO_y and Cl_x systems. ''OH may be a well-behaved constituent under a wide range of circumstances, as must be assumed in models in absence of measurements to the contrary, but it is essential that this assumption be tested.''

The simultaneous measurements of H_2O, cirrus ice content, temperature, O_3, CO, and N_2O in the region of the tropopause should improve our understanding of exchange processes between the stratosphere and troposphere. The MLS measurements are especially important in the Tropics where they can be made in the presence of cirrus, which can degrade techniques operating at ultraviolet, visible, and infrared wavelengths.

c. EOS MLS measurements for upper-tropospheric chemistry

EOS measurements in the upper troposphere include H_2O, O_3, CO, N_2O, HCl, ice content of dense cirrus, temperature, and pressure. The simultaneous measurement of O_3, and of CO, which serves as a tracer of air-mass origin and motion, should provide new information on the global distribution, variation, and sources of O_3 in the upper troposphere. Some of the larger variations expected in upper-tropospheric O_3 and CO due to biomass burning (e.g., Thompson et al. 1996; Pickering et al. 1996) should be detectable in daily maps from EOS MLS but smaller variations will require maps built up from averages of observations over a longer period of time. Cirrus clouds near the tropopause can potentially lead to the activation of chlorine and ozone loss (Bormann et al. 1996); models of this process (Solomon et al. 1997) fall short of explaining the pronounced minima in upper-tropospheric O_3 detected in the presence of ice clouds by ground-based lidar (Reichardt et al. 1996). EOS MLS should help to understand such phenomena on a global scale since it concurrently measures O_3 and cirrus ice, as well as CO, which can likely help identify regions of convective uplift where low O_3 might be due to dynamics, and N_2O and HCl, which can help identify air of stratospheric origin and provide estimates of the amount of inorganic chlorine available for activation by heterogeneous chemistry. The improved EOS MLS ability to measure stratospheric ozone column, over that of *UARS* MLS, should lead to better determinations of tropospheric ozone obtained from residuals between total column ozone measured by other sensors and the stratospheric column from EOS MLS.

d. EOS MLS measurements for climate variability studies

EOS MLS measurements relevant to climate variability studies include H_2O, cloud ice content, temperature, and O_3. The MLS measurements of H_2O in the upper troposphere are expected to be especially valuable because of uncertainties in climate feedback mechanisms associated with upper-tropospheric H_2O (e.g., Lindzen 1990) and the ability of MLS to provide such measurements in the presence of cirrus and with good vertical resolution. Some of the more interesting phenomena related to climate variability and feedback are associated with the behavior of upper-tropospheric water vapor in and around regions of deep convection in the Tropics, where the presence of cirrus can degrade measurements by shorter-wavelength techniques. The simultaneous MLS measurements of water in both the vapor and ice phases, along with temperature (and CO as a possible tracer of air motion), should provide new information on processes that affect formation of cirrus ice particles, which can have important climatic effects. The MLS temperature measurements complement those from infrared techniques in not being affected by variations in stratospheric aerosol content or CO_2, and complement those from nadir-looking microwave techniques in having better vertical (but poorer horizontal) resolution.

Acknowledgments. We thank many colleagues, too numerous to mention here by name, who have contributed so much to our experiments. Special thanks are due F. T. Barath for managing the *UARS* MLS instrument development, M. A. Frerking for leading the development of its JPL radiometers, and G. E. Peckham and colleagues involved with the U.K. portion of the *UARS* instrument. Particular thanks also to E. A. Cohen and colleagues for laboratory spectroscopy support, and R. E. Newell, R. B. Rood, R. J. Salawitch, B. J. Sandor, and M. R. Schoeberl for helpful discussions, and E. M. Stone for assistance in preparing Fig. 15. This work was performed at the California Institute of Technology Jet Propulsion Laboratory under contract with the U.S. National Aeronautics and Space Administration and at the University of Edinburgh Department of Meteorology under contract with the U.K. National Environmental Research Council.

REFERENCES

Aellig, C. P., and Coauthors, 1996: Latitudinal distribution of upper stratospheric ClO as derived from space borne microwave spectroscopy. *Geophys. Res. Lett.,* **23,** 2321–2324.

Alexander, M. J., 1997: A model of non-stationary gravity waves in the stratosphere and comparison to observations. *Gravity Wave Processes and Their Parameterization in Global Climate Models,* K. Hamilton, Ed., NATO ASI Series 1, Vol. 50, Springer-Verlag, 153–168.

Allen, D. R., J. L. Stanford, L. S. Elson, E. F. Fishbein, L. Froidevaux, and J. W. Waters, 1997: The 4-day wave as observed from the *Upper Atmosphere Research Satellite* Microwave Limb Sounder. *J. Atmos. Sci.,* **54,** 420–434.

Barath, F. T., and Coauthors, 1993: The Upper Atmosphere Research Satellite Microwave Limb Sounder instrument. *J. Geophys. Res.,* **98,** 10 751–10 762.

Bell, W., N. A. Martin, T. D. Gardiner, N. R. Swann, P. T. Woods, P. F. Fogal, and J. W. Waters, 1994: Column measurements of stratospheric trace species over Åre, Sweden in the winter of 1991–92. *Geophys. Res. Lett.,* **21,** 1347–1350.

Borrman, S., S. Solomon, J. E. Dye, and B. Luo, 1996: The potential of cirrus clouds for heterogeneous chlorine activation. *Geophys. Res. Lett.,* **23,** 2133–2136.

Canziani, P. O., J. R. Holton, E. F. Fishbein, L. Froidevaux, and J. W. Waters, 1994: Equatorial Kelvin waves: A *UARS* MLS view. *J. Atmos. Sci.,* **51,** 3053–3076.

——, ——, ——, ——, and ——, 1995: Equatorial Kelvin wave variability during 1992 and 1993. *J. Geophys. Res.,* **100,** 5193–5202.

Carr, E. S., and Coauthors, 1995: Tropical stratospheric water vapor measured by the Microwave Limb Sounder (MLS). *Geophys. Res. Lett.,* **22,** 691–694.

Chance, K. V., D. G. Johnson, W. A. Traub, and K. W. Jucks, 1991: Measurements of the stratospheric hydrogen peroxide profile using far infrared thermal emission spectroscopy. *Geophys. Res. Lett.,* **18,** 1003–1006.

Chandra, S., L. Froidevaux, J. W. Waters, O. R. White, G. J. Rottman, D. K. Prinz, J. W. Waters, and G. E. Brueckner, 1996: Ozone variability in the upper stratosphere during the declining phase of solar cycle 22. *Geophys. Res. Lett.,* **23,** 2935–2938.

Chen, M., R. B. Rood, and W. G. Read, 1998: Upper tropospheric water vapor from GEOS reanalysis and *UARS* MLS observations. *J. Geophys. Res.,* **103,** 19 587–19 594.

Chiou, E. W., M. P. McCormick, and W. P. Chu, 1997: Global water vapor distributions in the stratosphere and upper troposphere derived from 5.5 years of SAGE II observations (1986–1991). *J. Geophys. Res.,* **102,** 19 105–19 118.

Chipperfield, M., 1993: Satellite maps ozone destroyer. *Nature,* **362,** 592–593.

——, M. L. Santee, L. Froidevaux, G. L. Manney, W. G. Read, J. W. Waters, A. E. Roche, and J. M. Russell, 1996: Analyses of UARS data in the southern polar vortex in September 1992 using a chemical transport model. *J. Geophys. Res.,* **101,** 18 861–18 881.

Clark, H. L., R. S. Harwood, W. G. Read, and P. W. Mote, 1998: Tropical variability of upper tropospheric water vapour from the Microwave Limb Sounder on the Upper Atmosphere Research Satellite. *J. Geophys. Res.,* in press.

Crewell, S., R. Fabian, K. Künzi, H. Nett, T. Wehr, W. Read, and J. Waters, 1995: Comparison of ClO measurements made by airborne and spaceborne microwave radiometers in the Arctic winter stratosphere 1993. *Geophys. Res. Lett.,* **22,** 1489–1492.

Considine, D. B., A. E. Dessler, C. H. Jackman, J. E. Rosenfield, P. E. Mead, M. R. Schoeberl, A. E. Roche, and J. W. Waters, 1998: Interhemispheric assymmetry in the 1 mbar O_3 trend: An analysis using an interactive zonal mean model and UARS data. *J. Geophys. Res.,* **103,** 1607–1618.

Cunnold, D., H. Wang, W. P. Chu, and L. Froidevaux, 1996a: Comparisons between Stratospheric Aerosol and Gas Experiment II and microwave limb sounder ozone measurements and aliasing of SAGE II ozone trends in the lower stratosphere. *J. Geophys. Res.,* **101,** 10 061–10 075.

——, L. Froidevaux, J. M. Russell, B. Connor, and A. Roche, 1996b: Overview of UARS ozone validation based primarily on intercomparisons among UARS and Stratospheric Aerosol and Gas Experiment II measurements. *J. Geophys. Res.,* **101,** 10 335–10 350.

Dessler, A. E., and Coauthors, 1995: Correlated observations of HCl and $ClONO_2$ from UARS and implications for stratospheric chlorine partitioning. *Geophys. Res. Lett.,* **22,** 1721–1724.

——, and Coauthors, 1996a: A test of the partitioning between ClO and $ClONO_2$ using simultaneous UARS measurements of ClO, NO_2 and $ClONO_2$. *J. Geophys. Res.,* **101,** 12 515–12 521.

——, S. R. Kawa, D. B. Considine, J. W. Waters, L. Froidevaux, and J. B. Kumer, 1996b: UARS measurements of ClO and NO_2 at 40 and 46 km and implications for the 'ozone deficit.' *Geophys. Res. Lett.,* **23,** 339–342.

——, and Coauthors, 1998: Selected science highlights from the first five years of the Upper Atmosphere Research Satellite (UARS) program. *Rev. Geophys.,* **36,** 183–210.

Douglass, A., and Coauthors, 1993: A 3D simulation of the early winter distribution of reactive chlorine in the north polar vortex. *Geophys. Res. Lett.,* **20,** 1271–1274.

——, M. R. Schoeberl, R. S. Stolarski, J. W. Waters, J. M. Russell III, and A. E. Roche, 1995: Interhemispheric differences in springtime production of HCl and $ClONO_2$ in the polar vortices. *J. Geophys. Res.,* **100,** 13 967–13 978.

Eckman, R. S., and Coauthors, 1995: Stratospheric trace constituents simulated by a three-dimensional general circulation model: Comparison with UARS data. *J. Geophys. Res.,* **100,** 13 951–13 966.

Elson, L. S., and L. Froidevaux, 1993: The use of Fourier transforms for asynoptic mapping: Early results from the Upper Atmosphere Research Satellite Microwave Limb Sounder. *J. Geophys. Res.,* **98,** 23 039–23 049.

——, G. L. Manney, L. Froidevaux, and J. W. Waters, 1994: Large-scale variations in ozone from the first two years of *UARS* MLS data. *J. Atmos. Sci.,* **51,** 2867–2876.

——, W. G. Read, J. W. Waters, P. W. Mote, J. S. Kinnersley, and R. S. Harwood, 1996: Space-time variations in water vapor as observed by the UARS Microwave Limb Sounder. *J. Geophys. Res.,* **101,** 9001–9015.

Eluszkiewicz, J., and Coauthors, 1996: Residual circulation in the stratosphere and lower mesosphere as diagnosed from Microwave Limb Sounder data. *J. Atmos Sci.,* **53,** 217–240.

Evans, K. F., and G. L. Stephens, 1995: Microwave radiative transfer through clouds composed of realistically shaped ice crystals. Part I: Single scattering properties. *J. Atmos. Sci.,* **52,** 2041–2057.

——, S. J. Walter, A. J. Heymsfield, and M. N. Deeter, 1998: Modeling of submillimeter passive remote sensing of cirrus clouds. *J. Appl. Meteor.,* **37,** 184–205.

Fishbein, E. F., L. S. Elson, L. Froidevaux, G. L. Manney, W. G. Read, J. W. Waters, and R. W. Zurek, 1993: MLS observations of stratospheric waves in temperature and O_3 during the 1992 southern winter. *Geophys. Res. Lett.,* **20,** 1255–1258.

——, and Coauthors, 1996: Validation of UARS Microwave Limb Sounder temperature and pressure measurements. *J. Geophys. Res.,* **101,** 9938–10 016.

Froidevaux, L., J. W. Waters, W. G. Read, L. S. Elson, W. G. Read, D. A. Flower, and R. F. Jarnot, 1994: Global ozone observations from *UARS* MLS: An overview of zonal mean results. *J. Atmos. Sci.,* **51,** 2846–2866.

——, and Coauthors, 1996: Validation of UARS Microwave Limb Sounder ozone measurements. *J. Geophys. Res.,* **101,** 10 017–10 060.

Geller, M. A., Y. Chi, R. B. Rood, A. R. Douglass, D. J. Allen, M. Cerniglia, and J. W. Waters, 1993: 3-D transport-chemistry studies of the stratosphere using satellite data together with data assimilation. *The Role of the Stratosphere in Global Change,* M.-L. Chanin, Ed., NATO ASI Series, Vol. 18, Springler-Verlag, 179–198.

Haas, M. R., and L. Phister, 1998: A high-altitude site survey for Sofia. *Pub. Astron. Soc. Pacific,* **110,** 339–364.

——, V. Yudin, A. R. Douglass, J. W. Waters, L. S. Elson, A. E. Roche, and J. M. Russell, 1995: UARS PSC, $ClONO_2$, HCl, and ClO measurements in early winter: Additional verification of the paradigm for chlorine activation. *Geophys. Res. Lett.,* **22,** 2937–2940.

Hartmann, G. K., and Coauthors, 1996: Measurements of O_3, H_2O and ClO in the middle atmosphere using the millimeter-wave atmospheric sounder (MAS). *Geophys. Res. Lett.,* **23,** 2313–2316.

Harwood, R. S., and Coauthors, 1993: Springtime stratospheric water vapour in the southern hemisphere as measured by MLS. *Geophys. Res. Lett.,* **20,** 1235–1238.

Hofmann, D. J., 1996: Recovery of antarctic ozone hole. *Nature,* **384,** 222–223.

Hood, L. L., and S. Zhou, 1998: Stratospheric effects of 27-day solar ultraviolet variations: An analysis of UARS MLS ozone and temperature data. *J. Geophys. Res.,* **103,** 3629–3638.

Hu, H., and W. T. Liu, 1998: The impact of upper tropospheric humidity from Microwave Limb Sounder on the midlatitude greenhouse effect. *Geophys. Res. Lett.,* **25,** 3151–3154.

Huang, F. T., C. A. Reber, and J. Austin, 1997: Ozone diurnal variations observed by UARS and their model simulation. *J. Geophys. Res.,* **102,** 12 971–12 985.

Jackman, C. H., E. L. Fleming, S. Chandra, D. B. Considine, and J. E. Rosenfield, 1996: Past, present, and future modeled ozone trends with comparisons to observed trends. *J. Geophys. Res.,* **101,** 28 753–28 767.

Jarnot, R. F., R. E. Cofield, J. W. Waters, G. E. Peckham, and D. A. Flower, 1996: Calibration of the Microwave Limb Sounder on the Upper Atmosphere Research Satellite. *J. Geophys. Res.,* **101,** 9957–9982.

Khosravi, R., G. P. Brasseur, A. K. Smith, D. W. Rusch, J. W. Waters, and J. M. Russell III, 1998: Significant reduction in stratospheric ozone deficit using a 3-D model constrained with UARS data. *J. Geophys. Res.,* **103,** 16 203–16 219.

Kumer, J. B., J. L. Mergenthaler, and A. E. Roche, 1993: CLAES CH_4, N_2O and CCl_2F_2 global data. *Geophys. Res. Lett.,* **20,** 1239–1242.

Lahoz, W. A., and Coauthors, 1993: Northern Hemisphere mid-stratosphere vortex processes diagnosed from H_2O, N_2O and potential vorticity. *Geophys. Res. Lett.,* **23,** 2671–2674.

——, and Coauthors, 1994: Three-dimensional evolution of water vapor distributions in the Northern Hemisphere as observed by MLS. *J. Atmos. Sci.,* **51,** 2914–2930.

——, and Coauthors, 1996a: Validation of UARS Microwave Limb Sounder 183 GHz H_2O measurements. *J. Geophys. Res.,* **101,** 10 129–10 149.

——, and Coauthors, 1996b: Vortex dynamics and the evolution of water vapour in the stratosphere of the southern hemisphere. *Quart. J. Roy. Meteor. Soc.,* **122,** 423–450.

Lau, C. L., G. E. Peckham, R. A. Suttie, and R. F. Jarnot, 1996: Characterisation of MLS 1/f noise parameters. *Int. J. Remote Sens.,* **17,** 3751–3759.

Lefèvre, F., G. P. Brasseur, I. Folkins, A. K. Smith, and P. Simon, 1994: Chemistry of the 1991–92 stratospheric winter: Three-dimensional model simulations. *J. Geophys. Res.,* **99,** 8183–8195.

Limpasuvan, V., and C. B. Leovy, 1995: Observations of the two-day wave near the southern summer stratopause. *Geophys. Res. Lett.,* **22,** 2385–2388.

Lindzen, R. S., 1990: Some coolness concerning global warming. *Bull. Amer. Meteor. Soc.,* **71,** 288–299.

Lipson, J. B., M. J. Elrod, T. W. Beiderhase, L. T. Molina, and M. J. Molina, 1997: Temperature dependence of the rate constant and branching ratio for the OH + ClO reaction. *J. Chem. Soc. Faraday Trans.,* **93,** 2665–2673.

Lutman, E. R., J. A. Pyle, M. P. Chipperfield, D. J. Lary, I. Kilbane-Dawe, J. W. Waters, and N. Larsen, 1997: Three dimensional studies of the 1991/92 Northern Hemisphere winter using domain-filling trajectories with chemistry. *J. Geophys. Res.,* **102,** 1479–1488.

Mackenzie, I., R. S. Harwood, L. Froidevaux, W. G. Read, and J. W. Waters, 1996: Chemical loss of polar vortex ozone inferred from UARS MLS measurements of ClO during the Arctic and Antarctic springs of 1993. *J. Geophys. Res.,* **101,** 14 505–14 518.

Madden, R. A., and P. R. Julian, 1971: Detection of a 40–50 day oscillation in the zonal wind in the tropical Pacific. *J. Atmos. Sci.,* **28,** 702–708.

Manney, G. L., L. Froidevaux, J. W. Waters, L. S. Elson, E. F. Fishbein, R. W. Zurek, R. S. Harwood, and W. A. Lahoz, 1993: The evolution of ozone observed by UARS MLS in the 1992 late winter southern polar vortex. *Geophys. Res. Lett.,* **20,** 1279–1282.

——, and Coauthors, 1994: Chemical depletion of ozone in the Arctic lower stratosphere during winter 1992–93. *Nature,* **370,** 429–434.

——, R. W. Zurek, L. Froidevaux, and J. W. Waters, 1995a: Evidence for arctic ozone depletion in late February and early March 1994. *Geophys. Res. Lett.,* **22,** 2941–2944.

——, L. Froidevaux, J. W. Waters, and R. W. Zurek, 1995b: Evolution of microwave limb sounder ozone and the polar vortex during winter. *J. Geophys. Res.,* **100,** 2953–2972.

——, and Coauthors, 1995c: Formation of low ozone pockets in the middle stratosphere anticyclone during winter. *J. Geophys. Res.,* **100,** 13 939–13 950.

——, and Coauthors, 1995d: Lagrangian transport calculations using *UARS* data. Part I: Passive tracers. *J. Atmos. Sci.,* **52,** 3049–3068.

——, R. W. Zurek, L. Froidevaux, J. W. Waters, A. O'Neill, and R. Swinbank, 1995e: Lagrangian transport calculations using UARS data. Part II: Ozone. *J. Atmos. Sci.,* **52,** 3069–3081.

——, L. Froidevaux, J. W. Waters, M. L. Santee, W. G. Read, D. A. Flower, R. F. Jarnot, and R. W. Zurek, 1996a: Arctic ozone depletion observed by UARS MLS during the 1994–95 winter. *Geophys. Res. Lett.,* **23,** 85–88.

——, M. L. Santee, L. Froidevaux, J. W. Waters, and R. W. Zurek, 1996b: Polar vortex conditions during the 1995–96 arctic winter: Meteorology and MLS ozone. *Geophys. Res. Lett.,* **23,** 3203–3206.

——, L. Froidevaux, M. L. Santee, R. W. Zurek, and J. W. Waters, 1997: MLS observations of Arctic ozone loss in 1996–97. *Geophys. Res. Lett.,* **24,** 2687–2700.

——, J. C. Bird, D. P. Donovan, T. J. Duck, J. A. Whiteway, S. R. Pal, and A. I. Carswell, 1998a: Modelling ozone laminae in ground-based Arctic wintertime observations using trajectory calculations and satellite data. *J. Geophys. Res.,* **103,** 5797–5814.

——, J. Orsolini, H. C. Pumphrey, and A. E. Roche, 1998b: The 4-day wave and transport of *UARS* tracers in the austral polar vortex. *J. Atmos. Sci.,* **55,** 3456–3470.

Massie, S. T., and Coauthors, 1997: Simultaneous observations of polar stratospheric clouds and HNO_3 over Scandinavia in January, 1992. *Geophys. Res. Lett.,* **24,** 595–598.

Morrey, M. W., and R. S. Harwood, 1998: Interhemispheric differences in stratospheric water vapour during late winter, in version 4 MLS measurements. *Geophys. Res. Lett.,* **25,** 147–150.

Morris, G. A., and Coauthors, 1995: Trajectory mapping of Upper Atmosphere Research Satellite (UARS) data. *J. Geophys. Res.,* **100,** 16 491–16 505.

——, S. R. Kawa, A. R. Douglass, M. R. Schoeberl, L. Froidevaux, and J. W. Waters, 1998: Low ozone pockets explained. *J. Geophys. Res.,* **103,** 3599–3610.

Mote, P. W., K. H. Rosenlof, J. R. Holton, R. S. Harwood, and J. W. Waters, 1995: Seasonal variation of water vapour in the tropical lower stratosphere. *Geophys. Res. Lett.,* **22,** 1093–1096.

——, and Coauthors, 1996: An atmospheric tape recorder: The imprint of tropical tropopause temperatures on stratospheric water vapor. *J. Geophys. Res.,* **101,** 3989–4006.

——, T. J. Dunkerton, and H. C. Pumphrey, 1998: Sub-seasonal variations in lower stratospheric water vapor. *Geophys. Res. Lett.,* **25,** 2445–2448.

Nair, H., M. Allen, L. Froidevaux, and R. W. Zurek, 1998: Localized rapid ozone loss in the northern winter stratosphere: An analysis of UARS observations. *J. Geophys. Res.,* **103,** 1555–1571.

Newell, R. E., Y. Zhu, E. V. Browell, S. Ismail, W. G. Read, J. W. Waters, K. K. Kelly, and S. C. Liu, 1996a: Upper tropospheric water vapor and cirrus: Comparison of DC-8 observations, preliminary UARS microwave limb sounder measurements and meteorological analyses. *J. Geophys. Res.,* **101,** 1931–1941.

——, ——, ——, W. G. Read, and J. W. Waters, 1996b: Walker circulation and tropical upper tropospheric water vapor. *J. Geophys. Res.,* **101,** 1961–1974.

——, ——, W. G. Read, and J. W. Waters, 1997: Relationship between tropical upper tropospheric moisture and eastern tropical Pacific sea surface temperature at seasonal and interannual time scales. *Geophys. Res. Lett.,* **24,** 25–28.

Oh, J. J., and E. A. Cohen, 1992: Pressure broadening of ozone lines near 184 and 206 GHz by nitrogen and oxygen. *J. Quant. Spectrosc. Radiat. Transfer,* **48,** 405–408.

——, and ——, 1994: Pressure broadening of ClO by N_2 and O_2 near 204 and 649 GHz and new frequency measurements between 632 and 725 GHz. *J. Quant. Spectrosc. Radiat. Transfer,* **54,** 151–156.

Orsolini, Y. J., G. Hansen, U. Hoppe, G. L. Manney, and K. Fricke, 1997: Dynamical modelling of wintertime lidar observations in the arctic: Ozone laminae and ozone depletion. *Quart. J. Roy. Meteor. Soc.,* **123,** 785–800.

——, G. L. Manney, A. Engel, J. Ovarlez, C. Claud, and L. Coy, 1998: Layering in stratospheric profiles of long-lived trace species: Balloon-borne observations and modeling. *J. Geophys. Res.,* **103,** 5815–5825.

Pickering, K. E., and Coauthors, 1996: Convective transport of biomass burning emissions over Brazil during TRACE A. *J. Geophys. Res.,* **101,** 23 993–24 012.

Pickett, H. M., D. E. Brinza, and E. A. Cohen, 1981: Pressure broadening of ClO by nitrogen. *J. Geophys. Res.,* **86,** 7279–7282.

——, R. L. Poynter, and E. A. Cohen, 1992: Submillimeter, millimeter and microwave spectral line catalog. Tech. Rep. 80-23, Rev. 3, Jet Propulsion Lab., Pasadena, CA, 217 pp. [Avaiable from Jet Propulsion Laboratory, Pasadena, CA 91109-8099.]

Pumphrey, H. C., 1998: Nonlinear retrievals of water vapor from the UARS Microwave Limb Sounder (MLS). *Adv. Space. Res.,* **21** (3), 389–392.

——, and R. S. Harwood, 1997: Water vapour and ozone in the mesosphere as measured by UARS MLS. *Geophys. Res. Lett.,* **24,** 1399–2002.

Randel, W. J., J. C. Gille, A. E. Roche, J. B. Kumer, J. L. Mergenthaler, J. W. Waters, E. F. Fishbein, and W. A. Lahoz, 1993: Stratospheric transport from the tropics to middle latitudes by planetary-wave mixing. *Nature,* **365,** 533–535.

——, F. Wu, J. M. Russell III, J. W. Waters, and L. Froidevaux, 1995:

Ozone and temperature changes in the stratosphere following the eruption of Mount Pinatubo. *J. Geophys. Res.,* **100,** 16 753–16 754.

——, ——, ——, A. Roche, and J. W. Waters, 1998: Seasonal cycles and QBO variations in stratospheric CH_4 and H_2O observed in *UARS* HALOE data. *J. Atmos. Sci.,* **55,** 163–185.

Ray, E., J. R. Holton, E. F. Fishbein, L. Froidevaux, and J. W. Waters, 1994: The tropical semiannual oscillation in temperature and ozone observed by the MLS. *J. Atmos. Sci.,* **51,** 3045–3052.

Read, W. G., L. Froidevaux, and J. W. Waters, 1993: Microwave Limb Sounder (MLS) measurements of SO_2 from Mt. Pinatubo volcano. *Geophys. Res. Lett.,* **20,** 1299–1302.

——, J. W. Waters, L. Froidevaux, D. A. Flower, R. F. Jarnot, D. L. Hartmann, R. S. Harwood, and R. B. Rood, 1995: Upper-tropospheric water vapor from UARS MLS. *Bull. Amer. Meteor. Soc.,* **76,** 2381–2389.

Reber, C. A., 1993: The Upper Atmosphere Research Satellite (UARS). *Geophys. Res. Lett.,* **20,** 1215–1218.

——, C. E. Trevathan, R. J. McNeal, and M. R. Luther, 1993: The Upper Atmosphere Research Satellite (UARS) mission. *J. Geophys. Res.,* **98,** 10 643–10 647.

Redaelli, G., and Coauthors, 1994: UARS MLS O_3 soundings compared with lidar measurements using the conservative coordinates reconstruction technique. *Geophys. Res. Lett.,* **21,** 1535–1538.

Reichardt, J., A. Ansmann, M. Serwazi, C. Weitkamp, and W. Michaelis, 1996: Unexpectedly low ozone concentration in midlatitude tropospheric ice clouds: A case study. *Geophys. Res. Lett.,* **23,** 1929–1932.

Ricaud, P., and Coauthors, 1995: Polar stratospheric clouds as deduced from MLS and CLAES measurements. *Geophys. Res. Lett.,* **22,** 2033–2036.

——, J. de La Noë, B. J. Connor, L. Froidevaux, J. W. Waters, R. S. Harwood, I. A. MacKenzie, and G. E. Peckham, 1996: Diurnal variability of mesospheric ozone as measured by the UARS microwave limb sounder instrument: Theoretical and ground-based validations. *J. Geophys. Res.,* **101,** 10 077–10 089.

——, and Coauthors, 1998: The stratosphere over Dumont d'Urville, Antarctica, in winter 1992. *J. Geophys. Res.,* **103,** 13 267–13 284.

Roche, A. E., J. B. Kumer, J. L. Mergenthaler, G. A. Ely, W. G. Uplinger, J. F. Potter, T. C. James, and L. W. Sterrit, 1993: The Cryogenic Limb Array Etalon Spectrometer (CLAES) on UARS: Experiment description and performance. *J. Geophys. Res.,* **98,** 10 763–10 775.

Rood, R. B., A. R. Douglass, M. C. Cerniglia, and W. G. Read, 1997: Synoptic-scale mass exchange from the troposphere to the stratosphere. *J. Geophys. Res.,* **102,** 23 467–23 485.

Roscoe, H. K., A. E. Jones, and A. M. Lee, 1997: Midwinter start to Antarctic ozone depletion: Evidence from observations and models. *Science,* **278,** 93–96.

Rosenlof, K. H., 1995: Seasonal cycle of the residual mean meridional circulation in the stratosphere. *J. Geophys. Res.,* **100,** 5173–5191.

Rottman, G. J., T. N. Woods, and T. P. Sparn, 1993: Solar-stellar irradiance comparison experiment 1. Instrument design and operation. *J. Geophys. Res.,* **98,** 10 667–10 677.

Russell, J. M., III, and Coauthors, 1993: The Halogen Occultation Experiment. *J. Geophys. Res.,* **98,** 10 777–10 797.

Salawitch, R. J., 1998: Ozone depletion: A greenhouse warming connection. *Nature,* **392,** 551–552.

Sandor, B. J., W. G. Read, J. W. Waters, and K. H. Rosenlof, 1998: Seasonal behavior of tropical to mid-latitude upper tropospheric water vapor from UARS MLS. *J. Geophys. Res.,* **103,** 25 935–25 947.

Santee, M. L., and Coauthors, 1995: Interhemispheric differences in polar stratospheric HNO_3, H_2O, ClO and O_3. *Science,* **267,** 849–852.

——, and Coauthors, 1996a: Chlorine deactivation in the lower stratospheric polar regions during late winter: Results from UARS. *J. Geophys. Res.,* **101,** 18 835–18 859.

——, G. L. Manney, W. G. Read, L. Froidevaux, and J. W. Waters, 1996b: Polar vortex conditions during the 1995–96 arctic winter: MLS ClO and HNO_3. *Geophys. Res. Lett.,* **23,** 3207–3210.

——, ——, L. Froidevaux, R. W. Zurek, and J. W. Waters, 1997: MLS observations of ClO and HNO_3 in the 1996–97 Arctic polar vortex. *Geophys. Res. Lett.,* **24,** 2713–2716.

——, A. Tabazedeh, G. L. Manney, R. J. Salawitch, L. Froidevaux, W. G. Read, and J. W. Waters, 1998: UARS MLS HNO_3 observations: Implications for Antarctic PSCs. *J. Geophys. Res.,* **103,** 13 285–13 314.

Schoeberl, M. R., R. S. Stolarski, A. R. Douglass, P. A. Newman, L. R. Lait, J. W. Waters, L. Froidevaux, and W. G. Read, 1993: MLS ClO observations and arctic polar vortex temperatures. *Geophys. Res. Lett.,* **20,** 2861–2864.

——, and Coauthors, 1996: The development of the Antarctic ozone hole. *J. Geophys. Res.,* **101,** 20 909–20 924.

——, A. E. Roche, J. M. Russell III, D. Ortland, P. B. Hays, and J. W. Waters, 1997: An estimation of the dynamical isolation of the tropical lower stratosphere using UARS wind and trace gas observations of the quasi-biennial oscillation. *Geophys. Res. Lett.,* **24,** 53–56.

Shindell, D. T., D. Rind, and P. Lonergan, 1998: Increased polar stratospheric ozone losses and delayed eventual recovery owing to increasing greenhouse gas concentrations. *Nature,* **392,** 589–592.

Siegel, P. H., and Coauthors, 1993: Heterodyne radiometer development for the Earth Observing System Microwave Limb Sounder. *Infrared and Millimeter-Wave Engineering,* H. Buscher, Ed., SPIE Vol. 1874, 124–137.

Singh, U. N., and Coauthors, 1996: Stratospheric temperature measurements by two collocated NDSC lidar during UARS validation campaign. *J. Geophys. Res.,* **101,** 10 287–10 297.

Solomon, S., and R. R. Garcia, 1984: On the distributions of long-lived tracers and chlorine species in the middle atmosphere. *J. Geophys. Res.,* **89,** 11 633–11 644.

——, S. Borrmann, R. R. Garcia, R. Portmann, L. Thomason, L. R. Poole, D. Winker, and M. P. McCormick, 1997: Heterogeneous chlorine chemistry in the tropopause region. *J. Geophys. Res.,* **102,** 21 411–21 429.

Spencer, R. W., and W. D. Braswell, 1997: How dry is the tropical free troposphere? Implications for global warming theory. *Bull. Amer. Meteor. Soc.,* **78,** 1097–1106.

Stachnik, R. A., J. C. Hardy, J. A. Tarsala, J. W. Waters, and N. R. Erickson, 1992: Submillimeterwave heterodyne measurements of stratospheric ClO, HCl, O_3, and HO_2: First results. *Geophys. Res. Lett.,* **19,** 1931–1934.

Stone, E. M., and Coauthors, 1995: Space-time integrity of improved stratospheric and mesospheric sounder and microwave limb sounder temperature fields at Kelvin wave scales. *J. Geophys. Res.,* **100,** 14 089–14 096.

——, W. J. Randel, J. L. Stanford, W. G. Read, and J. W. Waters, 1996: Baroclinic wave variations observed in MLS upper tropospheric water vapor. *Geophys. Res. Lett.,* **23,** 2967–2970.

Tabazadeh, A., R. P. Turco, K. Drdla, M. Z. Jacobsen, and O. B. Toon, 1994: A study of type I polar stratospheric cloud formation. *Geophys. Res. Lett.,* **21,** 1619–1622.

Taylor, F. W., and Coauthors, 1993: Remote sensing of atmospheric structure and composition by pressure modulator radiometry from space: The ISAMS experiment on UARS. *J. Geophys. Res.,* **98,** 10 799–10 814.

Thompson, A. M., and Coauthors, 1996: Where did tropospheric ozone over southern Africa and the tropical Atlantic come from in October 1992? Insights from TOMS, GTE TRACE A, and SAFARI 1992. *J. Geophys. Res.,* **101,** 24 251–24 278.

Toumi, R., and S. Bekki, 1993: The importance of the reactions between OH and ClO for stratospheric ozone. *Geophys. Res. Lett.,* **20,** 2447–2450.

Waters, J. W., 1989: Microwave limb-sounding of Earth's upper atmosphere. *Atmos. Res.,* **23,** 391–410.

——, 1992a: Submillimeter heterodyne spectroscopy and remote sensing of the upper atmosphere. *IEEE Proc.,* **80,** 1679–1701.

——, 1992b: Submillimeter heterodyne spectroscopy and remote sensing of the upper atmosphere. *The Use of EOS for Studies of Atmospheric Physics,* J. C. Gille and G. Visconti, Eds., Elsevier, 491–579.

——, 1993: Microwave limb sounding. *Atmospheric Remote Sensing by Microwave Radiometry,* M. A. Janssen, Ed., John Wiley, 383–496.

——, 1997: The Upper Atmosphere Research Satellite (UARS). *The Stratosphere and Its Role in the Climate System,* G. P. Brasseur, Ed., NATO ASI Series 1, Vol. 54, Springer-Verlag, 345–365.

——, 1998: Atmospheric measurements by the MLS experiments: Results from UARS and plans for the future. *Adv. Space Res.,* **21** (10), 1363–1372.

——, and Coauthors, 1979: Aircraft search for millimeter wavelength emission by stratospheric ClO. *J. Geophys. Res.,* **84,** 6934.

——, J. J. Gustincic, P. N. Swanson, and A. R. Kerr, 1980: Measurements of upper atmospheric H_2O emission at 183 GHz. *Atmospheric Water Vapor,* A. Deepak, T. Wilkerson, and L. Ruhnke, Eds., Academic Press, 229–240.

——, J. C. Hardy, R. F. Jarnot, and H. M. Pickett, 1981: Chlorine monoxide radical, ozone, and hydrogen peroxide: Stratospheric measurements by microwave limb sounding. *Science,* **214,** 61–64.

——, ——, ——, ——, and P. Zimmermann, 1984: A balloon-borne microwave limb sounder for stratospheric measurements. *J. Quant. Spectrosc. Radiat. Transfer,* **32,** 407–433.

——, R. A. Stachnik, J. C. Hardy, and R. F. Jarnot, 1988: ClO and O_3 stratospheric profiles: Balloon microwave measurements. *Geophys. Res. Lett.,* **15,** 780–783.

——, L. Froidevaux, G. L. Manney, W. G. Read, and L. S. Elson, 1993a: Lower stratospheric ClO and O_3 in the 1992 southern hemisphere winter. *Geophys. Res. Lett.,* **20,** 1219–1222.

——, ——, W. G. Read, G. L. Manney, L. S. Elson, D. A. Flower, R. F. Jarnot, and R. S. Harwood, 1993b: Stratospheric ClO and ozone from the Microwave Limb Sounder on the Upper Atmosphere Research Satellite. *Nature,* **362,** 597–602.

——, G. L. Manney, W. G. Read, L. Froidevaux, D. A. Flower, and R. F. Jarnot, 1995: UARS MLS observations of lower stratospheric ClO in the 1992–93 and 1993–94 arctic winter vortices. *Geophys. Res. Lett.,* **22,** 823–826.

——, and Coauthors, 1996: Validation of UARS Microwave Limb Sounder ClO measurements. *J. Geophys. Res.,* **101,** 10 091–10 127.

Weinreb, S., 1997: Millimeter-wave integrated-circuit radiometers. *Passive Millimeter-Wave Technology,* R. M. Smith, Ed., SPIE, Vol. 3064, 80–89.

——, P. C. Chao, and W. Copp, 1997: Full waveguide band, 90 to 140 GHz MMIC amplifier module. *1997 IEEE MTT-S Digest,* 1279–1280.

Wild, J. D., and Coauthors, 1995: Comparison of stratospheric temperature from several lidars, using National Meteorological Center and Microwave Limb Sounder data as transfer references. *J. Geophys. Res.,* **100,** 11 105–11 111.

Wu, D. L., and J. W. Waters, 1996a: Gravity-wave-scale temperature fluctuations seen by the UARS MLS. *Geophys. Res. Lett.,* **23,** 3289–3292.

——, and ——, 1996b: Satellite observations of atmospheric variances: A possible indication of gravity waves. *Geophys. Res. Lett.,* **23,** 3631–3634.

——, and ——, 1997: Observations of gravity waves with the UARS Microwave Limb Sounder. *Gravity Wave Processes and Their Parameterization in Global Climate Models,* K. Hamilton, Ed., NATO ASI Series, Vol. 50, Springler-Verlag, 103–120.

——, E. F. Fishbein, W. G. Read, and J. W. Waters, 1996: Excitation and evolution of the quasi 2-day wave observed in *UARS*/MLS temperature measurements. *J. Atmos. Sci.,* **53,** 728–738.

——, C. McLandress, E. F. Fishbein, W. G. Read, J. W. Waters, and L. Froidevaux, 1998: Equatorial diurnal variations observed in UARS Microwave Limb Sounder temperature during 1991–1994 and simulated by the Canadian Middle Atmosphere Model. *J. Geophys. Res.,* **103,** 8909–8917.

Ziemke, J. R., S. Chandra, A. M. Thompson, and D. P. McNamara, 1996: Zonal asymmetries in southern hemisphere column ozone: Implications of biomass burning. *J. Geophys. Res.,* **101,** 14 421–14 427.